

Zero-shot Forecasting by Simulation Alone

Boris N. Oreshkin¹, Mayank Jauhari¹, Ravi Kiran Selvam¹, Malcolm Wolff¹, Wenhao Pan^{1,4},
 Shankar Ramasubramanian¹, Kin G. Olivares¹, Tatiana Konstantinova¹, Andres Potapczynski^{1,3},
 Mengfei Cao¹, Dmitry Efimov¹, Michael W. Mahoney^{1,2}, Andrew G. Wilson^{1,3}
 oreshkin@amazon.com

¹Amazon, ²UC Berkeley, ³New York University, ⁴University of Washington

Abstract

Zero-shot time-series forecasting holds great promise, but is still in its infancy, hindered by limited and biased data corpora, leakage-prone evaluation, and privacy and licensing constraints. Motivated by these challenges, we propose the first practical univariate time series simulation pipeline which is simultaneously fast enough for on-the-fly data generation and enables notable zero-shot forecasting performance on M-Series and GiftEval benchmarks that capture trend/seasonality/intermittency patterns, typical of industrial forecasting applications across a variety of domains. Our simulator, which we call **SarSim0 (SARIMA Simulator for Zero-Shot Forecasting)**, is based off of a seasonal autoregressive integrated moving average (SARIMA) model as its core data source. Due to instability in the autoregressive component, naive SARIMA simulation often leads to unusable paths. Instead, we follow a three-step procedure: (1) we sample well-behaved trajectories from its characteristic polynomial stability region; (2) we introduce a superposition scheme that combines multiple paths into rich multi-seasonality traces; and (3) we add rate-based heavy-tailed noise models to capture burstiness and intermittency alongside seasonalities and trends. **SarSim0** is orders of magnitude faster than kernel-based generators, and it enables training on *circa* 1B unique *purely simulated* series, generated on the fly; after which well-established neural network backbones exhibit strong zero-shot generalization, surpassing strong statistical forecasters and recent foundation baselines, while operating under strict zero-shot protocol. Notably, on GiftEval we observe a “student-beats-teacher” effect: models trained on our simulations exceed the forecasting accuracy of the **AutoARIMA** generating processes.

1 Introduction

Zero-shot learning fixes a pretrained model and predicts on target data with no parameter updates. While this paradigm has reshaped natural language processing and computer vision (Yosinski et al., 2014; Wei et al., 2022), zero-shot time series forecasting is still in its infancy, but it is rapidly gaining interest. Indeed, zero-shot forecasting (Garza & Mergenthaler-Canseco, 2023; Gruver et al., 2023) offers compelling advantages for deployment scenarios, *e.g.*, because using a frozen pre-trained model eliminates target-side selection loops and tuning heuristics. By collapsing rollout to pure inference—no backpropagation, no per-dataset adaptation—zero-shot forecasting meets tight latency and cost envelopes, and it simplifies platform optimization (train once, reuse everywhere), while lowering compute and energy budgets per forecast. It also aligns with privacy and governance constraints: inference on sensitive targets remains strictly local, with no gradient flow or parameter updates that could leak information, easing compliance and audits. While recent work in time series forecasting focuses on architectural novelty (Liang et al., 2024), data is the lifeblood of zero-shot prediction. Curated compilations of real series can be helpful, but they inevitably run into problems, including licensing barriers, limited scale, and domain and cadence biases. Most problematic for zero-shot integrity is *leakage*: overlapping datasets in train/test, as well as target-side hyperparameter search confound evaluation. Using just synthetic data has shown promise for zero-shot forecasting, but it has not yet been able to fully substitute for real data. For example, Ansari et al. (2024) show that augmenting real data with a kernel-based synthetic generation procedure yields better results than using real data alone; however, they find training solely

on synthetic data can significantly degrade performance; and Kuvshinova et al. (2024) find that zero-shot pretraining on synthetic data is not comparable relative to using even a small amount of real data.

In this paper, our goal is to bridge this gap and develop an effective synthetic-only training pipeline for zero-shot time series forecasting. Synthetic data offers unique levers: controllable coverage of seasonalities and sampling rates, programmatic rare events, debiasing, and guaranteed leakage-free generation—things that real compilations cannot easily match. Building on this premise, we provide the following contributions in this work. (1) We propose `SarSim0`, a fast three-stage synthetic time series simulator (see Figure 1) that produces rich, realistic patterns and that is efficient enough to synthesize sequences on-the-fly, thereby enabling pretraining at the scale of billions of series. To start, we first sample stable poles of the characteristic polynomial of a seasonal auto-regressive integrated moving average (SARIMA) process (Section 4.1). SARIMA provides a natural choice as our simulator backbone both because it is deeply rooted in stochastic time series modeling, and because it is fast and expressive, subsuming many other time series models as special cases (Hyndman et al., 2025). We also show that it captures the fidelity of real time series data with rich structure (Figure 3). Then, we introduce a superposition scheme, combining sample paths for multi-seasonality via modulation (Section 4.2). Finally, we add rate-based heavy-tailed noise models to capture burstiness and intermittency (Section 4.3). (2) We provide a detailed empirical evaluation of `SarSim0` (Section 5) on the M-Series (Makridakis et al., 1982; Makridakis & Hibon, 2000; Makridakis et al., 2020; Athanasopoulos et al., 2011) and GiftEval (Aksu et al., 2024) benchmarks. Our scope is zero-shot forecasting in industrial settings, where series are largely driven by complex trend, seasonality, and intermittency / heavy-tail patterns. M-Series and GiftEval, which span multiple domains (Nature, Web/CloudOps, Sales, Energy, Transport, Healthcare, Demographic, Finance, Industry, Macro/Micro Economic) and frequencies (yearly, quarterly, monthly, weekly, daily, hourly, and some sub-hourly), provide a comprehensive testbed for this regime. We find that training exclusively on time series generated by our simulator yields compact, fast, and accurate models that generalize across these zero-shot benchmarks under a strict no-leakage guarantee. We show that, on these benchmarks, simulated data can be competitive with, or even outperform, real-data pretraining, substantially closing the gap between small efficient architectures and large foundation models; and on GiftEval, we see evidence for a “student beats teacher” generalization behavior. On the more regular, relatively short and low-noise business and macroeconomic M-Series, this effect is mixed, with `AutoARIMA` remaining very strong. This indicates that such emergent generalization is dataset- and domain-dependent, and is currently most pronounced on more heterogeneous and noisier benchmarks like GiftEval.

2 Background

Univariate quantile forecasting. Let $y_{1:t} \in \mathbb{R}^t$ be a univariate time series observed up to time t , and let H be the forecast horizon. We aim to predict, for each forecast horizon $h = 1, \dots, H$, a set of Q conditional quantiles of y_{t+h} . We fix quantile levels $\boldsymbol{\tau} := (\tau_1, \dots, \tau_Q)$, $0 < \tau_1 < \dots < \tau_Q < 1$, and we define a lookback (context) window of length $\ell < T$, $\mathbf{x}_t := y_{t-\ell+1:t} \in \mathbb{R}^\ell$, and forecasting model, $\mathcal{F}_\psi : \mathbb{R}^\ell \rightarrow \mathbb{R}^{H \times Q}$, producing quantile matrix, $\mathbf{x}_t \mapsto \widehat{\mathbf{Y}}_{T+1:T+H}^{(\boldsymbol{\tau})}$, with elements $\widehat{y}_{t+h}^{(\boldsymbol{\tau})}$.

Learning via Empirical Risk Minimization (ERM) with multi-horizon, multi-quantile loss. From a training corpus, we extract N supervised examples by rolling windows across one or more univariate series, $\mathcal{D} = \{(\mathbf{x}_{t_i}, y_{t_i+1:t_i+H})\}_{i=1}^N$. We further define the quantile loss at level τ as:

$$\rho_\tau(y, \hat{y}) = \tau(y - \hat{y})_+ + (1 - \tau)(\hat{y} - y)_+ \quad \text{with} \quad u_+ := \max\{u, 0\}.$$

The multi-horizon, multi-quantile loss for a single example i is:

$$\mathcal{L}_{H,Q}(y_{T+1:T+H}, \widehat{\mathbf{Y}}_{T+1:T+H}^{(\boldsymbol{\tau})}) := \frac{1}{HQ} \sum_{h=1}^H \sum_{\tau \in \boldsymbol{\tau}} \rho_\tau(y_{T+h}, \widehat{y}_{T+h}^{(\boldsymbol{\tau})}). \quad (1)$$

The ERM objective optimizing the network parameters ψ to approximate the conditional quantile function $\tau \mapsto F_{y_{t+h}|\mathbf{x}_t}^{-1}(\tau)$ on the grid $\boldsymbol{\tau}$ uniformly over horizons $h = 1, \dots, H$ is then given by:

$$\psi^* \in \arg \min_{\psi \in \Psi} \frac{1}{N} \sum_{(\mathbf{x}, \mathbf{y}) \in \mathcal{D}} \mathcal{L}_{H,Q}(\mathbf{y}, \mathcal{F}_\psi(\mathbf{x})).$$

Zero-shot forecasting. By *zero-shot forecasting*, we mean that we freeze all model parameters after pre-training on a source corpus, and we then condition on a target series to make forecasts, while keeping the model parameters frozen. More precisely, following the definition of the zero-shot forecasting task from Oreshkin et al. (2021), let $\mathcal{D}^{(S)}$ be a *source* training corpus and let $\mathcal{D}^{(T)}$ be a *target* test corpus constructed from series disjoint from $\mathcal{D}^{(S)}$ (no entity, segment, or time-window overlap). A forecasting model \mathcal{F}_ψ is first trained on $\mathcal{D}^{(S)}$ (and, if needed, all model selection is performed using splits of $\mathcal{D}^{(S)}$ only), yielding parameters ψ^* . *Zero-shot evaluation* on $\mathcal{D}^{(T)}$ proceeds by applying the *frozen* (weights, normalizers, embeddings) predictor \mathcal{F}_{ψ^*} to each target series independently, *one at a time*, using only the available lookback window for that series at each prediction time.

3 Related Work

Transfer Learning. Early approaches to transfer learning in forecasting focused on frequency-specialized models (*i.e.*, one model for monthly frequency, one model for quarterly frequency, etc). Success was measured by the model’s ability to outperform statistical baselines: **AutoARIMA** (Hyndman & Khandakar, 2008), **ETS** (Holt, 1957), and **Theta** (Fiorucci et al., 2016), when applied to large time series corpora. Progress in this area has been driven by adopting cross-learning via training of global models on large time series collections to extract shared patterns; and this approach underpins the success of top-performing models in competitions like **M4** and **M5** (Smil, 2019; Anderer & Li, 2022), as well as industry models such as **DeepAR**, **MQCNN** and **TFT** (Salinas et al., 2020; Wen et al., 2017; Lim et al., 2021). Zero-shot forecasting in time series emerged from transfer-learning formulations such as (Oreshkin et al., 2021), which showed that a frequency-specific source-trained model can be deployed to unseen series without target-side updates.

Foundation Models. Subsequent work moves beyond frequency-specific forecasters toward foundation-style pretraining, leveraging large sequence models for zero-shot prediction. **TimeGPT** (Garza & Mergenthaler-Canseco, 2023) pioneered the use of pre-trained transformers for forecasting, and **LLMTime** (Gruver et al., 2023) extended this approach by adapting **Llama** (Touvron et al., 2023). **TimesFM** adopts patch tokens and a decoder-only backbone for fast multi-step generation (Das et al., 2024); **MOIRAI** (Woo et al., 2024) couples patching with any-variate projections and mixture-likelihood heads for cross-frequency robustness; and **LagLlama** retains a decoder-only design with lag features and parametric distribution heads (Rasul et al., 2024). **Chronos** adopts a different approach by quantizing series values and uses encoder-decoder LMs with next-token cross-entropy for probabilistic decoding (Ansari et al., 2024). Beyond attention, **TTM** targets accuracy-latency Pareto efficiency with all-MLP mixers (Ekambaram et al., 2024). Recent work has highlighted subtle and non-obvious tradeoffs as training knobs are varied for different classes of models (Yu et al., 2025b;a).

Synthetic time series data. **ForecastPFN** (Dooley et al., 2023) generates synthetic training corpora by composing simple priors over trend and seasonal components, combined with multiplicative Weibull noise. **KernelSynth** from **Chronos** (Ansari et al., 2024) augments real datasets with GP-kernel-based synthetic samples. **TimePFN** (Taga et al., 2025) extends these approaches to multivariate settings using GP-kernel compositions and channel mixing. Unlike other approaches, our simulator is grounded in stochastic time series dynamics (stable SARIMA) with broad expressive power (complemented with hierarchical seasonality and heavy-tailed noisers) rather than hand-crafted seasonal-trend templates or slow kernel synthesis. This yields high-fidelity temporal dependence, heteroscedasticity, and burstiness, while remaining orders of magnitude faster. Consequently, we pretrain foundation models *exclusively* on simulated data at scale; the resulting models exhibit strong zero-shot generalization across heterogeneous benchmarks, surpassing results of prior synthetic approaches (*e.g.*, **ForecastPFN**, **KernelSynth**).

4 SarSim0: time series Simulator Pipeline

A central hypothesis of this work is that high-quality synthetic data can unlock scalable pretraining for zero-shot forecasting. In domains such as computer vision and natural language processing, foundation models are fueled by massive, diverse corpora. Time series, by contrast, suffer from (relatively) limited public datasets, licensing constraints, and pervasive risks of statistical leakage. A realistic, efficient simulator offers an alternative path: it enables pretraining at scale while guaranteeing leakage-free evaluation. To this end, we propose a modular simulation pipeline, which we call **SarSim0** (**SARIMA Simulator** for **Zero-Shot**

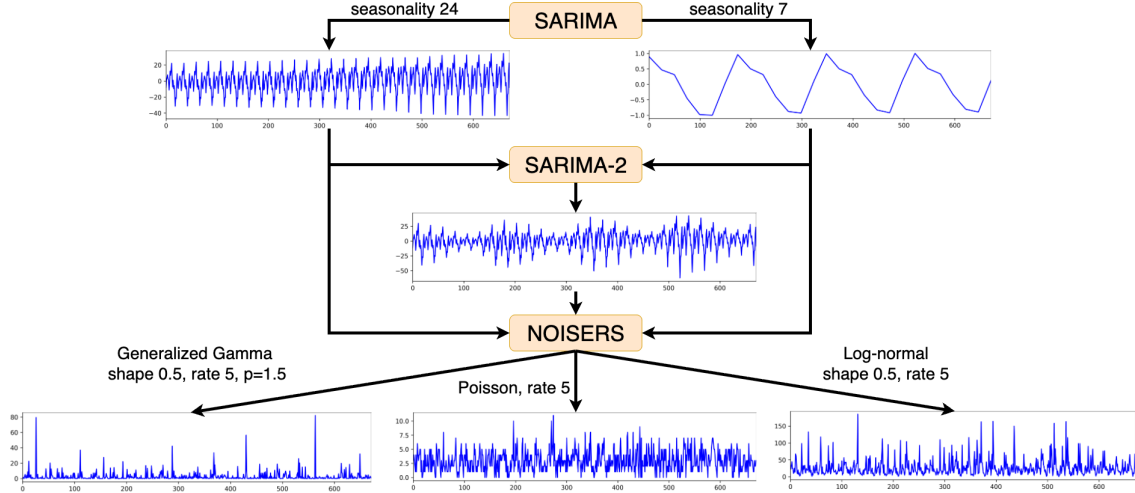


Figure 1: **SarSim0 simulator pipeline.** Top: two base components are generated by SARIMA with AR (and seasonal) roots sampled via the characteristic polynomial inside the stability region, yielding well-behaved paths at seasonalities $s=24$ and $s=7$. Middle: a SARIMA-2 superposition/modulation block combines the components to produce a double-seasonal series with rich cross-frequency structure. Bottom: a noise module injects heavy-tailed disturbances: *e.g.*, Poisson spikes, generalized-gamma bursts, and log-normal volatility capturing burstiness, intermittency, and realistic deviations from Gaussian noise.

Forecasting). **SarSim0** can be formalized as:

$$y_{1:T} = \mathbb{N} \circ \mathbb{I} \circ \mathbb{S}(\epsilon). \quad (2)$$

Here \mathbb{S} is a structured base-signal generator, \mathbb{I} is the interaction component that consumes tuples of structured signals and composes them into richer waveforms via parameterized interaction patterns (*e.g.*, additive mixing or multiplicative modulation); and \mathbb{N} overlays the structured output with stochastic perturbations, including heavy-tailed noise to capture burstiness and intermittency. The overall **SarSim0** system diagram, along with generated examples is shown in Figure 1. The design is guided by three requirements for effective pretraining: (i) structural fidelity to recurring motifs in real series (seasonality, trends, intermittency); (ii) scalability to billions of samples without storage overhead; and (iii) diversity sufficient to support generalization across heterogeneous benchmarks.

In this paper, for the base generator of **SarSim0**, we adopt SARIMA, because it combines deep statistical time series grounding with broad expressive power and computational efficiency. First, SARIMA subsumes many statistical models as special cases: it recovers Simple Exponential Smoothing, linear trend and seasonal Holt’s method, as well as damped-trend Holt-Winters variant (Hyndman et al., 2025). Additionally, random walk (Naïve), seasonal Naïve, Airline model (Box et al., 2015), and **Theta** method (Hyndman & Billah, 2003a) formulations are all nested within the SARIMA family, making it a unifying lens for widely adopted forecasting approaches (Hyndman et al., 2025). Second, SARIMA underlies the **AutoARIMA** procedure (Hyndman & Khandakar, 2008), which remains one of the strongest zero-shot baselines in forecasting competitions and applied practice. By grounding **SarSim0** in SARIMA, we inherit the statistical foundations of classical models and retain a direct link to **AutoARIMA** as a natural “teacher”, while aligning with and complementing the inductive biases of neural “student” architectures. We will see that **SarSim0**-trained models outperform **AutoARIMA**; moreover, as Figure 3 shows, SARIMA reproduces the statistical structure of real-world time series, providing a credible training signal.

4.1 SARIMA Simulator

Without loss of generality, we start the exposition with the *Auto-Regressive Moving Average* (ARMA) process of order p', q that can be defined as:

$$y_t - \alpha_1 y_{t-1} - \cdots - \alpha_{p'} y_{t-p'} = \varepsilon_t + \vartheta_1 \varepsilon_{t-1} + \cdots + \vartheta_{q'} \varepsilon_{t-q}. \quad (3)$$

Here $\alpha_{1:p'}$ are auto-regressive coefficients, $\vartheta_{1:q}$ are moving average coefficients, and $\varepsilon_{t-q:t}$ are zero-mean i.i.d. innovations. With the lag operator L defined as $L y_t = y_{t-1}$, this process can be written compactly in

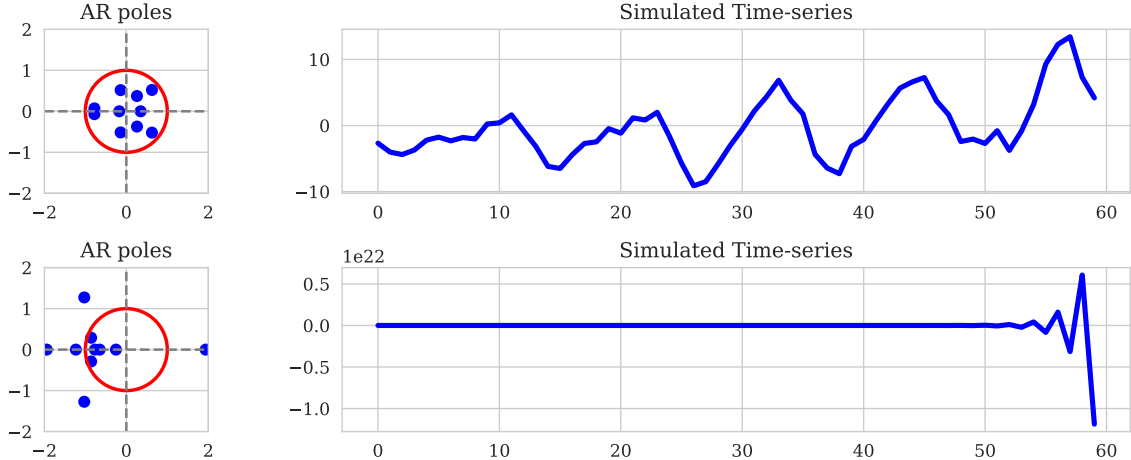


Figure 2: **Sampling of SARIMA poles by SarSim0.** The SARIMA order-10 AR process poles are shown along with the unit circle on the left. The resulting generated processes with these poles are shown on the right. The top pane shows poles sampled according to the proposed procedure, resulting in a realistic looking time series. The bottom pane shows the result of unconstrained random generation of AR coefficients, resulting in a divergent time series that is useless from the perspective of training time series foundation models.

polynomial form:

$$\left(1 - \sum_{i=1}^p \phi_i L^i\right) (1 - L)^d y_t = \left(1 + \sum_{i=1}^q \vartheta_i L^i\right) \varepsilon_t, \quad (4)$$

where $p = p' - d$ and coefficients ϕ are derived from coefficients α to factor out d unit roots of the polynomial, corresponding to the finite difference time domain integrator, $y_t \leftarrow y_t + y_{t-1}$. Consequently, ARMA with integrator ($d > 0$) is called ARIMA (integrated ARMA).

In principle, ARIMA could be used directly as a time series simulator, by randomly generating initial state y_0 , orders p', q ; coefficients α, ϑ ; excitation noise ε , and unrolling Equation (3) through time. However, as shown in Figure 2 (bottom), setting the coefficients arbitrarily destabilizes the system and results in divergent nonsensical time series that are not useful for training a forecasting model. To circumvent this stability issue, we propose instead to operate directly in the model's pole space, guaranteeing valid process dynamics by construction. In particular, there is a link between the summation-based polynomial form (4) and the product-based pole representation:

$$\phi(L) = 1 - \sum_{i=1}^p \phi_i L^i = \prod_{i=1}^p (1 - \varphi_i L). \quad (5)$$

Well-behavedness of the AR part is guaranteed if the poles, φ_i , lie within unit circle, $|\varphi_i| < 1$, (Hamilton, 1994, Chapter 3). Thus, we propose to sample the poles of the AR and MA transfer functions, $\{\varphi_i\}_{i=1}^p$ and $\{\vartheta_j\}_{j=1}^q$ respectively, and then derive the system coefficients α and ϑ from the pole representation using product expansion (e.g., numpy's np.poly). A typical realization of the process sampled using this approach is shown in Figure 2 (top). In contrast to Figure 2 (bottom), all poles of the AR system are located within unit circle, resulting in a well-behaved simulation result.

To complete the polynomial specification of the base SARIMA, we include the seasonal part with parameters s (period), D (integration order), P (seasonal AR order), Q (seasonal MA order):

$$\left(1 - \sum_{i=1}^p \phi_i L^i - \sum_{j=1}^P \Phi_j L^{js}\right) (1 - L)^d (1 - L^s)^D y_t = \left(1 + \sum_{i=1}^q \vartheta_i L^i + \sum_{j=1}^Q \Theta_j L^{js}\right) \varepsilon_t.$$

We note that the AR side is the *joint* lacunary (sparse) polynomial $A(L) = 1 - \sum_{i=1}^p \phi_i L^i - \sum_{j=1}^P \Phi_j (L^s)^j$. In the additive form, joint stability is non-factorizable: A does not split into independent nonseasonal and

seasonal factors. This nonseparability, together with the gappy support $\{1, \dots, p\} \cup \{s, 2s, \dots, Ps\}$, makes the stability region nonconvex and numerically thin: small changes in (ϕ, Φ) can move poles across the unit circle, especially near seasonal frequencies. Therefore, to obtain well-behaved simulations, we adopt a mixture approach: with probability 0.5 we draw an AR-only model ($\Phi_j = 0$ for all j) and with probability 0.5 a seasonal-AR-only model ($\phi_i = 0$ for all i); each subcase is trivial to stabilize.

These considerations lead to the following practical algorithm for sampling a general SARIMA process. First, sample model orders p, q, P, Q uniformly at random (from 0 to the maximum integer value defined for each of them). For the AR side, flip a fair coin and set either $p = 0$ or $P = 0$ with probability 0.5. Then, once the model order is defined, sample poles uniformly within the unit circle by first sampling the radius uniformly between 0 and r_{\max} and then the complex angle in $[0, 2\pi]$. Next, convert roots to coefficients by expanding the poles product into polynomial form (*e.g.*, see Equation 5)); we also set the integration order to $d = 1$ and $D = 1$, since higher integration orders tend to be numerically unstable. Finally, sample the warmup trajectory state $y_{1:w}$ and innovations process $\varepsilon_{1:w}$ from i.i.d. zero-mean normal distribution, setting $w = \max(p, q, P \cdot s, Q \cdot s, d + D \cdot s)$, and unroll the SARIMA process according to the following time-domain recursion starting at $t = w + 1$:

$$y_t = \sum_{i=1}^p \phi_i y_{t-i} + \sum_{j=1}^P \Phi_j y_{t-j \cdot s} + \sum_{i=1}^q \vartheta_i \varepsilon_{t-i} + \sum_{j=1}^Q \Theta_j \varepsilon_{t-j \cdot s} + \varepsilon_t. \quad (6)$$

We apply the non-seasonal and seasonal integrators as a separate pass ($y_t \leftarrow y_t + y_{t-1}$, $y_t \leftarrow y_t + y_{t-s}$). To produce more diverse trend patterns, we further enrich the integration framework by subjecting y_t to a fractional differencing operator, which results in simulating fractional integration orders between 0 and 1 (by sampling fractional difference order d' uniformly at random in $[0, 1]$). We approximate the fractional differencing operator by a finite impulse response filter with binomial coefficients, following the work of Hosking (1981): $\varrho_i = \Gamma(i - d')/(\Gamma(-d')\Gamma(i + 1))$. Simulating trajectories via the recursion (6) is reasonably fast, but the time dependence imposes a sequential loop that cannot be vectorized across *time*. To remove this bottleneck, we vectorize across trajectories: for each sampled parameter tuple p, q, P, Q, s, d' , we draw B independent sets of initial conditions (and innovations), and we unroll B paths in parallel. This delivers substantial speedups from vectorized computation and preserves diversity as distinct initial states yield diverse realizations under the same parameters.

4.2 SARIMA-2 Simulator

Many real-world series exhibit *bi-seasonality*: a fast rhythm modulated by a slower envelope. Examples include road traffic, web activity, call-center volumes (intra-day peaks modulated by weekday effects) (Moreira-Matias et al., 2013; Strowes, 2016; Ibrahim & L’Ecuyer, 2016); electric load (intraday cycles shaped by weekday and annual patterns) (Hong & Fan, 2016). Single-season models capture the fast cadence but miss amplitude modulation and the induced heteroscedasticity. These observations motivate a compositional construction with two seasonal processes: one high-frequency “base,” and one low-frequency “envelope,” whose additive or multiplicative interaction reproduces the envelope-on-carrier structure observed in practice. To model this structure, we introduce SARIMA-2, which composes two independent, pole-stable SARIMA processes: a high-frequency *base* series $y_t^{(b)}$, and a low-frequency *envelope* series $y_t^{(e)}$. The envelope is upsampled to the base rate and combined with the base either additively or multiplicatively:

$$\text{Additive: } y_t \leftarrow y_t^{(b)} + y_t^{(e)}, \quad (7)$$

$$\text{Multiplicative: } y_t \leftarrow (1 + \omega \tilde{y}_t^{(e)}) y_t^{(b)}, \quad (8)$$

where, in the multiplicative case, $\tilde{y}_t^{(e)}$ is normalized to $[-1, 1]$ and modulation depth, ω , is sampled from $\text{Uniform}(0, 1)$. This composition induces controlled amplitude modulation, capturing effects such as weekday intensity swings. We show an input-output pair for multiplicative SARIMA-2 in Figure 1 (middle).

4.3 Noisers

Many domains exhibit statistical features that cannot be captured by seasonal dynamics (that have a given time scale) alone. Retail and spare-parts demand often shows intermittent spikes and long runs

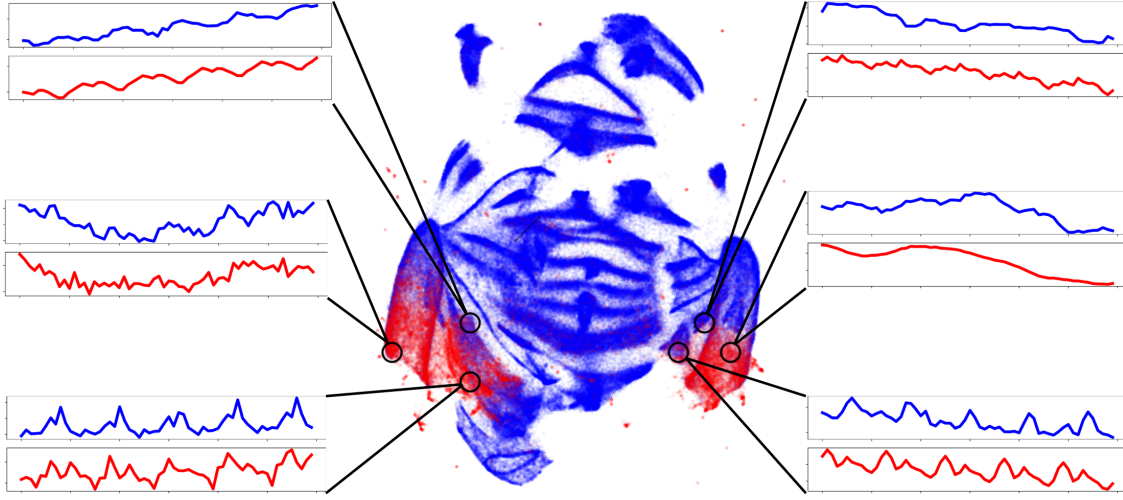


Figure 3: **SarSim0 Fidelity with Real time series Data.** Center: UMAP embedding space of 60-step windows from real dataset M4-Monthly (red) overlaid on equal-length samples from SARIMA simulator with uniformly sampled seasonality $s \in \{0, \dots, 24\}$ (blue). Left and right: real (red) and synthetic (blue) series drawn from the circled regions. Key take-aways include: (1) the simulator spans the seasonal regimes seen in real data (e.g., M4-Monthly), including the overall dataset as a special case; and (2) within a seasonality, synthetic series closely match real exemplars co-located in the embedding space, yielding realistic, fine-grained patterns.

of zeros, motivating Poisson- or count-based models (Croston, 1972; Syntetos & Boylan, 2005). Internet traffic and web workloads are well known to follow heavy-tailed distributions and exhibit burstiness across multiple time scales (Willinger et al., 1995; Feldmann et al., 1998). Environmental processes such as daily precipitation amounts are classically modeled with Gamma-family distributions, highlighting the need for positive, heavy-tailed shocks (Wilks, 1999; Ghil et al., 2002). Together, these examples establish that real-world series frequently combine heteroscedasticity, intermittency, and heavy-tailed disturbances with their seasonal structure. To capture these effects, our simulator incorporates a dedicated *Noiser* module, \mathbb{N} , which implements the random rate noise process:

$$\eta_t \sim \mathbb{N}_\kappa(\lambda_t), \quad \lambda_t = g(y_t) \geq 0,$$

where y_t is the structured signal (output of SARIMA or SARIMA-2), $g(\cdot)$ maps level to a time-varying *rate* (e.g., normalization plus a log-uniform scale), and κ denotes the distribution’s *shape* hyperparameter(s). The rate λ_t ties variability to the local mean level (heteroscedasticity), while κ governs the distributional form, typically controlling overdispersion and skew (e.g., for the Gamma distribution the coefficient of variation is $1/\sqrt{\kappa}$ (Johnson et al., 1994)). Thus, λ_t sets the scale of fluctuations conditional on y_t , and κ calibrates how those fluctuations are distributed (spread, asymmetry, and tail behavior). We implement three complementary noiser families: Poisson, Generalized Gamma and Lognormal. All noisers condition their variance on the local series level, normalized by series min and max values and scaled by the rate intensity sampled from LogUniform:

$$\lambda_t = \lambda_0(y_t - \min_t y_t) / (\max_t y_t - \min_t y_t), \quad \lambda_0 \sim \text{LogUniform}[\lambda_{\min}, \lambda_{\max}]. \quad (9)$$

Poisson noiser generates level-dependent count spikes characteristic of intermittent demand and arrivals, $\eta_t \sim \text{Poisson}(\lambda_t)$. *Generalized Gamma noiser* introduces controllable burstiness by sampling from a gamma distribution, $\eta'_t \sim \text{Gamma}(\lambda_t, \kappa)$, $\kappa \sim \text{LogUniform}[\kappa_{\min}, \kappa_{\max}]$, and further applying a random power transform $\eta_t = [\eta'_t]^\zeta$, $\zeta \sim \text{Uniform}[\zeta_{\min}, \zeta_{\max}]$. *Lognormal noiser* produces multiplicative, heavy-tailed shocks that emulate volatility fluctuations by sampling $\eta'_t \sim \text{LogNormal}(\lambda_t, \kappa)$, $\kappa \sim \text{LogUniform}[\kappa_{\min}, \kappa_{\max}]$. This combination provides a compact, simulator-friendly toolkit to reproduce the main classes of non-Gaussian, level-dependent disturbances observed in practice, while remaining efficient for large-scale, on-the-fly generation. The examples of noise traces produced by the three Noisers are provided in Figure 1 (bottom).

5 Empirical results

In this section, we evaluate `SarSim0` along five axes. (i) **Fidelity**: Do synthetic series reproduce the statistical structure of real data, providing a credible training signal? (ii) **Generalization**: Does pretraining on simulated data yield models that transfer zero-shot to heterogeneous real datasets, and how does performance compare to models pretrained on real data (*e.g.*, `Chronos`, `Moirai`, `TimesFM`)? (iii) **Architecture robustness**: Can architectures with distinct inductive biases, trained on synthetic diversity at scale, reach performance competitive with recent neural forecasters; and can diversity+scale substitute for architectural complexity? (iv) **Student-beats-teacher effects**: Do models trained only on simulated data outperform their “teacher” (*i.e.*, `AutoARIMA` derived from `SARIMA`) on real benchmarks? (v) **Ablations**: Do each of the proposed components, `SARIMA`, `SARIMA-2`, and the `Noisers`, contribute measurably to zero-shot generalization? We start by detailing benchmarks, baselines, training and testing protocols, followed by quantitative results and ablation studies addressing these questions.

5.1 Benchmarks

`GiftEval` is a curated benchmark for evaluating time series foundation models: models are applied to standardized test splits from 23 datasets spanning seven domains and ten sampling frequencies. The benchmark reports results for an array of statistical, deep, and foundation baselines (Aksu et al., 2024). The detailed composition of the benchmark and constituent datasets is provided in Appendix A.

M-Series is composed of four forecasting tasks comprising over 100,000 time series, curated from established forecasting competitions: **M1** (Makridakis et al., 1982), **M3** (Makridakis & Hibon, 2000), **M4** (Makridakis et al., 2020), and **Tourism** (Athanasopoulos et al., 2011). These datasets, summarized in Table 4 of Appendix B, represent a broad range of domains and temporal frequencies.

To ensure the comparability of our work with the existing literature, we evaluate the accuracy of the forecasts using well-established metrics: *scaled Continuous Ranked Probability Score* (sCRPS, (Gneiting & Raftery, 2007)), and *Mean Absolute Scaled Error* (MASE, (Hyndman & Koehler, 2006)), defined in Appendix D. M-Series results report average sCRPS and MASE across datasets weighted by dataset size. `GiftEval` results report geometric mean of sCRPS and MASE of each method divided by sCRPS and MASE of seasonal naive on each dataset (Aksu et al., 2024). Importantly, in both benchmarks, we use the datasets solely for evaluation purposes—excluding them from model optimization—to assess the zero-shot forecasting capabilities of our models.

5.2 Baselines and Training Methodology

We consider a collection of well-established baselines that includes `AutoARIMA` from `StatsForecast` (Garza et al., 2022). Neural forecasting baselines trained on the train splits of target datasets are represented by `NBEATS` (Oreshkin et al., 2020) and `PatchTST` (Nie et al., 2023). In terms of foundation models, we use publicly available pretrained checkpoints of `Chronos` (Ansari et al., 2024), `TimesFM` (Das et al., 2024), `MOIRAI` (Woo et al., 2024), and `TTM` (Ekambaram et al., 2024). Our proposed simulator is trained on `NBEATS`, `MLP` (a single block of `NBEATS`), `PatchTST` and `Chronos-Small T5`. These models represent very different types of inductive biases (fully-connected design vs. attention-based and patching designs) and all are generally accepted as strong baselines in the literature. Models are implemented in PyTorch (Paszke et al., 2019) and trained for 250k (`NBEATS`) and 500k (`PatchTST`, `Chronos`) steps. Models predict 512 horizons ahead in one shot. Further details and hyperparameter settings along with `SarSim0` simulator settings appear in Appendix E. In all cases, *trained models are applied at inference time with no tuning of parameters or hyperparameters on test datasets*. In addition, `NBEATS`, `PatchTST` and `Chronos` are trained on two baseline synthetic data generators, `ForecastPFN` (Dooley et al., 2023) and `KernelSynth` (Ansari et al., 2024) to assess `SarSim0`’s effectiveness w.r.t. existing methods. `ForecastPFN` training uses the exact same settings as `SarSim0`, whereas for `KernelSynth` we were only able to generate and save to disk up to 10M time series (which is 10 times the scale of synthetic data reported in (Ansari et al., 2024)) of length 1024 due to the very slow generation process (see Figure 4 in Appendix F for a speed comparison of synthetic pipelines).

5.3 Results

We begin by exploring the **fidelity** of the proposed `SARIMA`-based simulator in relation to real time series data. As an illustration, Figure 3 shows a joint UMAP of z-scored 48k windows (60 steps) from

	GiftEval		M-SERIES		Inference Time (m)	Zero-Shot
	sCRPS	MASE	sCRPS	MASE		
Chronos-Base	0.647	0.870	0.103	0.878	2103	✓
Chronos-Small	0.662	0.892	0.103	0.882	702	✓
MOIRAI-Large	0.599	0.874	0.128	1.027	3976	✓
MOIRAI-Small	0.650	0.946	0.124	1.089	994	✓
TTM-R2-Pretrained	0.873	1.020	0.155	1.118	43	✓
TimesFM	0.680	1.077	0.098	0.930	155	✓
NBEATS	0.815	0.937	0.095	1.134	271*	✗
PatchTST	0.587	0.848	0.090	1.613	165*	✗
AutoARIMA	0.912	1.074	0.096	0.843	420	✗
NBEATS-KernelSynth	0.686	0.978	0.116	1.033	-	✓
NBEATS-ForecastPFN	1.070	1.354	0.113	0.979	-	✓
PatchTST-KernelSynth	0.702	0.977	0.119	1.051	-	✓
PatchTST-ForecastPFN	1.060	1.346	0.105	0.949	-	✓
Chronos-KernelSynth	0.688	0.987	0.113	1.003	-	✓
Chronos-ForecastPFN	1.283	1.575	0.118	1.001	-	✓
NBEATS-SarSim0	0.602	0.849	0.096	0.869	46	✓
PatchTST-SarSim0	0.573	0.837	0.097	0.877	47	✓
Chronos-SarSim0	0.608	0.878	0.100	0.896	52	✓
MLP-SarSim0	0.643	0.907	0.109	0.982	45	✓

Table 1: **Performance on benchmarks, weighted aggregation over datasets.** Lower values are better. In the second block, AutoARIMA is fitted on each test series, while NBEATS and PatchTST are trained from scratch on the training split of each dataset (inference time with * includes training time). A green checkmark denotes models evaluated under a strict zero-shot protocol, a yellow checkmark denotes pretrain-test overlap (details in Appendix C), and a red cross denotes non-zero-shot baselines. Key take-aways include: (1) SarSim0 enables strong zero-shot forecasting from synthetic data alone, even outperforming real data pre-training; (2) SarSim0 outperforms alternative more expensive synthetic data pipelines, such as KernelSynth; (3) small models such as NBEATS with SarSim0 close the gap and even slightly exceed large models like Chronos; (4) on GiftEval, architectures pre-trained on SarSim0 outperform AutoARIMA derived from SARIMA generating process.

M4-Monthly, containing monthly time series rich with (a) trends and (b) monthly seasonalities with period 12 from demographic, finance, industry domains (Makridakis et al., 2020), and 384k equal-length SARIMA samples. Two features are particularly apparent. (i) *Seasonal strata*: Uniformly sampling the seasonal period $s \in \{0, \dots, 24\}$ yields blue clusters that align with s ; some align with the red M4 modes, indicating that SARIMA’s seasonal knob reproduces and *extends* the dominant structure of the real data. (ii) *Local co-location*: Within each stratum, real and synthetic windows are intermingled; because UMAP preserves local neighborhoods, intermingling suggests a match in short-lag autocovariances and narrowband peaks, not just marginals. Together with the side-panel look-alikes (instance-level fidelity), these observations make SARIMA a plausible data engine for pretraining forecasters capturing relevant seasonal modes, and reproducing local dynamics.

Our key results on **generalization** and **architecture robustness** appear in Table 1, showing aggregate metrics across two benchmarks. Models pretrained solely on our synthetic data achieve strong zero-shot generalization across heterogeneous benchmarks. In particular, NBEATS-SarSim0, PatchTST-SarSim0 and Chronos-SarSim0 consistently outperform their counterparts trained on prior synthetic approaches (KernelSynth, ForecastPFN); and they even more than close the gap to large real-data-pretrained models (*i.e.*, Chronos, MOIRAI, TimesFM, TTM-R2). The results support the claim that our simulator provides a sufficiently rich training signal to transfer across domains without exposure to target data. Moreover, the relative gains of NBEATS-SarSim0, PatchTST-SarSim0 and Chronos-SarSim0 highlight *architecture robustness*: architectures with distinct inductive biases reach competitive performance when trained on the same synthetic corpus. Together, these results suggest that diversity and scale of simulated series can partially complement and substitute for architectural complexity. Beyond aggregate scores, we stratify GiftEval results by domain, sampling frequency, term length, and variate type (Appendix H.3). Across all splits, SarSim0-pretrained backbones are consistently competitive with, and often stronger than, real-data foundation models. At the

	GiftEval		M-SERIES	
	sCRPS	MASE	sCRPS	MASE
PatchTST-SarSim0-500K	0.573	0.837	0.097	0.877
PatchTST-SarSim0-250K	0.576	0.838	0.102	0.922
No SARIMA-2-250K	0.647	0.926	0.103	0.929
No Noisers-250K	0.594	0.859	0.096	0.861
NBEATS-SarSim0	0.602	0.849	0.096	0.869
No SARIMA-2	0.655	0.913	0.104	0.941
No Noisers	0.609	0.856	0.096	0.860

Table 2: **SarSim0 ablation**, where lower values are better. Key take-aways include: (1) Removing SARIMA-2 causes the largest accuracy drop across backbones and benchmarks, positioning it as important generalization driver. (2) Removing Noisers has dataset- and model-dependent effects. For PatchTST and limited train budget of 250K iterations, this hurts on GiftEval, but it helps on the more regular M-Series. For extended training budget of 500K iterations, PatchTST with Noisers recovers performance on the M-Series, while retaining stronger results on GiftEval.

same time, **SarSim0** uniformly outperforms prior synthetic generators (KernelSynth, ForecastPFN) and often matches or surpasses strong per-dataset supervised **NBEATS**/**PatchTST** baselines. This indicates that a single, domain-agnostic SARIMA-based curriculum transfers robustly across GiftEval’s diverse regimes.

Table 1 also lets us probe a question: can models trained solely on synthetic trajectories derived from SARIMA exceed their statistical “teacher” (**AutoARIMA** derived from SARIMA) on real data? On GiftEval, **NBEATS-SarSim0**, **PatchTST-SarSim0** and **Chronos-SarSim0** achieve markedly *lower* sCRPS and MASE than **AutoARIMA**. On the M-series benchmark, the evidence is mixed. For example, **NBEATS-SarSim0** matches sCRPS, but it is slightly worse in MASE. Overall, despite being trained on SARIMA-generated data, these neural forecasters exhibit predictive capacity that extends beyond their generative teacher. While Table 1 is based on the full **SarSim0** (including SARIMA-2 and Noisers), which is not exactly expressible as a single **AutoARIMA** specification, Table 22 in Appendix H.4 shows that **NBEATS** trained *only* on pure SARIMA samples leads to the same qualitative conclusion.

Finally, we tackle the **Ablation** axes. Looking at Table 2 we conclude that removing SARIMA-2 (the interaction layer) causes the largest drop in zero-shot accuracy for both **PatchTST** and **NBEATS**, uniformly across benchmarks, suggesting it as a strong driver of generalization. Removing the Noisers has clear model- and benchmark-dependent effects. For PatchTST, for instance, we find that more iterations (500K vs. 250K) are needed to fully benefit from Noisers. This points to a practical trade-off: under tight compute budgets, a simpler simulator configuration and backbone may be preferable, whereas with more generous budgets, the full **SarSim0** pipeline and more expressive backbones yield, in our experiments, stronger overall zero-shot performance. In addition, we performed the **SarSim0** hyperparameter sensitivity study (see Table 13 in Appendix H.2 for details). Across studied configurations, performance on both GiftEval and the M-Series remains very similar to the default configuration, indicating that **SarSim0** is not at a brittle “sweet spot” in design space. The configuration we use (details in Appendix E.3) appears to be benchmark-agnostic and robust to substantial hyperparameter changes.

To probe behavior far outside our target regime of business-style series, we also ran a zero-shot experiment on four canonical nonlinear dynamical systems (Duffing, Lorenz, Lotka-Volterra, Pendulum), comparing several **Chronos** variants, **TimesFM**, and **SarSim0**-pretrained models (see Appendix H.1 for details). **SarSim0**-pretrained models attain error levels comparable to real-data foundation models. This suggests that **SarSim0**’s inductive biases, while geared toward trend/seasonality/intermittency regimes typical of industrial forecasting, yield models whose out-of-domain generalization is similar to that of real-data-pretrained models on these systems.

6 Discussion

By introducing **SarSim0**, we have shown that it is possible to achieve competitive zero-shot forecasting through training on simulated time series data alone. By enforcing stability in autoregressive pole sampling, introducing hierarchical seasonality through superposition, and overlaying heavy-tailed noise processes, our

SarSim0 simulator generates trajectories that are fast to generate, privacy- and license-safe, and sufficiently realistic to train models that generalize across real datasets. **Central findings.** First, on GiftEval and the M-Series, simulator-only pretraining achieves competitive zero-shot performance and sometimes exceeds real-data pretraining, suggesting that simulator fidelity, scale, and diversity can matter as much as architectural inductive biases. Second, we also see that our synthetic data pipeline can more than close the gap between small architectures and large pre-trained models such as **Chronos**, again highlighting the power of data generation. Additionally, on GiftEval we observe early, benchmark-specific evidence of a “student-beats-teacher” effect. Global neural models pretrained on **SarSim0**, whose core stochastic assumptions mirror the SARIMA family underlying **AutoARIMA**, can outperform this strong per-series **AutoARIMA** baseline. This suggests an emergent form of generalization beyond the simulator components, motivating further exploration of synthetic-first training for time series foundation models. **Limitations.** There are many exciting directions for future work. For example, Appendix G presents a novelty analysis comparing the SARIMA distributions against M4-monthly using a Local Outlier Factor detector. A consistent and interpretable pattern emerges among the most novel real windows: they typically exhibit (i) abrupt level shifts or structural breaks (*e.g.*, changes in trend slope or regime changes in the underlying process), and (ii) strong, isolated spikes or outages that do not repeat seasonally (especially isolated aperiodic negative spikes). This motivates natural extensions of **SarSim0** based on richer volatility and regime-switching structures (*e.g.*, GARCH-style components or regime-switching SARIMA), which we leave as important future work. While we expect hybrid synthetic-real training to outperform either source alone in many practical settings, we deliberately focus on the clean synthetic-only zero-shot regime, leaving synthetic-real co-training as an important direction for future work. Exogenous covariates are also not considered. Finally, it would be particularly fascinating to understand in detail when and why learners can surpass their generative teachers.

References

Taha Aksu, Gerald Woo, Juncheng Liu, Xu Liu, Chenghao Liu, Silvio Savarese, Caiming Xiong, and Doyen Sahoo. Gift-eval: A benchmark for general time series forecasting model evaluation. *arXiv preprint arXiv:2410.10393*, 2024. URL <https://arxiv.org/abs/2410.10393>.

Matthias Anderer and Feng Li. Hierarchical forecasting with a top-down alignment of independent-level forecasts. *International Journal of Forecasting*, 38(4):1405–1414, 2022. Special Issue: M5 competition.

Abdul Fatir Ansari, Lorenzo Stella, Caner Turkmen, Xiyuan Zhang, Pedro Mercado, Huibin Shen, Oleksandr Shchur, Syama Sundar Rangapuram, Sebastian Pineda Arango, Shubham Kapoor, Jasper Zschiegner, Danielle C. Maddix, Michael W. Mahoney, Kari Torkkola, Andrew Gordon Wilson, Michael Bohlke-Schneider, and Yuyang Wang. Chronos: Learning the language of time series, 2024.

George Athanasopoulos, Rob J. Hyndman, Haiyan Song, and Doris C. Wu. The tourism forecasting competition. *International Journal of Forecasting*, 27(3):822–844, 2011.

George E. P. Box, Gwilym M. Jenkins, Gregory C. Reinsel, and Greta M. Ljung. *Time Series Analysis: Forecasting and Control*. Wiley, 5 edition, 2015.

Markus M Breunig, Hans-Peter Kriegel, Raymond T Ng, and Jörg Sander. Lof: identifying density-based local outliers. In *Proceedings of the 2000 ACM SIGMOD international conference on Management of data*, pp. 93–104, 2000.

John D. Croston. Forecasting and stock control for intermittent demands. *Operational Research Quarterly*, 23(3):289–303, 1972.

Abhimanyu Das, Weihao Kong, Rajat Sen, and Yichen Zhou. A decoder-only foundation model for time-series forecasting, 2024. URL <https://arxiv.org/abs/2310.10688>.

Samuel Dooley, Gurnoor Singh Khurana, Chirag Mohapatra, Siddartha V Naidu, and Colin White. Forecastpfn: Synthetically-trained zero-shot forecasting. *Advances in Neural Information Processing Systems*, 36:2403–2426, 2023.

David Duvenaud, James Lloyd, Roger Grosse, Joshua Tenenbaum, and Ghahramani Zoubin. Structure discovery in nonparametric regression through compositional kernel search. In *International Conference on Machine Learning*, pp. 1166–1174. PMLR, 2013.

Vijay Ekambaram, Arindam Jati, Nam H. Nguyen, Pankaj Dayama, Chandra Reddy, Wesley M. Gifford, and Jayant Kalagnanam. Tiny Time Mixers (TTMs): Fast Pre-trained Models for Enhanced Zero/Few-Shot Forecasting of Multivariate Time Series, 2024. URL <https://arxiv.org/abs/2401.03955>.

William Falcon and The PyTorch Lightning team. PyTorch Lightning, March 2019. URL <https://github.com/Lightning-AI/lightning>.

Anja Feldmann, Anna C. Gilbert, Walter Willinger, and T. Kurtz. The changing nature of network traffic: Scaling phenomena. In *Computer Communication Review*, volume 28, pp. 5–29. ACM, 1998.

Jose A. Fiorucci, Tiago R. Pellegrini, Francisco Louzada, Fotios Petropoulos, and Anne B. Koehler. Models for optimising the theta method and their relationship to state space models. *International Journal of Forecasting*, 32(4):1151–1161, 2016.

Azul Garza and Max Mergenthaler-Canseco. Timegpt-1. *arXiv preprint arXiv:2310.03589*, 2023.

Federico Garza, Max Mergenthaler Canseco, Cristian Challú, and Kin G. Olivares. StatsForecast: Lightning fast forecasting with statistical and econometric models. PyCon Salt Lake City, Utah, US 2022, 2022. URL <https://github.com/Nixtla/statsforecast>.

Michael Ghil, Myles R. Allen, Michael D. Dettinger, Kerstin Ide, Dmitri Kondrashov, Michael E. Mann, Andrew W. Robertson, Andrea Saunders, Y. Tian, Ferenc Varadi, and Pascal Yiou. Advanced spectral methods for climatic time series. *Reviews of Geophysics*, 40(1):3–1–3–41, 2002.

Tilmann Gneiting and Adrian E Raftery. Strictly proper scoring rules, prediction, and estimation. *Journal of the American statistical Association*, 102(477):359–378, 2007.

Rakshitha Godahewa, Christoph Bergmeir, Geoffrey I. Webb, Rob J. Hyndman, and Pablo Montero-Manso. Monash time series forecasting archive. *CoRR*, abs/2105.06643, 2021. URL <https://arxiv.org/abs/2105.06643>.

Nate Gruver, Marc Finzi, Shikai Qiu, and Andrew Gordon Wilson. Large language models are zero-shot time series forecasters. In *Advances in Neural Information Processing Systems*, 2023. URL <https://arxiv.org/abs/2310.07820>.

James D. Hamilton. *Time Series Analysis*. Princeton University Press, Princeton, NJ, 1994.

Charles C Holt. Forecasting seasonals and trends by exponentially weighted moving averages. (*O.N.R. Memorandum No. 52*), 1957. URL <https://doi.org/10.1016/j.ijforecast.2003.09.015>.

Tao Hong and Shu Fan. Probabilistic electric load forecasting: A tutorial review. *International Journal of Forecasting*, 32(3):914–938, 2016.

J.R.M. Hosking. Fractional differencing. *Biometrika*, 68(1):165–176, 1981.

Addison Howard, Haruka Yui, Mark McDonald, and Will Cukierski. Recruit restaurant visitor forecasting. <https://www.kaggle.com/competitions/recruit-restaurant-visitor-forecasting>, 2017. Kaggle Competition.

Rob J. Hyndman and Baki Billah. Unmasking the theta method. *International Journal of Forecasting*, 19(2): 287–290, 2003a.

Rob J. Hyndman and Baki Billah. Unmasking the theta method. *International Journal of Forecasting*, 19(2): 287–290, 2003b.

Rob J. Hyndman and Yeasmin Khandakar. Automatic time series forecasting: The forecast package for r. *Journal of Statistical Software, Articles*, 27(3):1–22, 2008.

Rob J. Hyndman and Anne B. Koehler. Another look at measures of forecast accuracy. *International Journal of Forecasting*, 22(4):679 – 688, 2006.

Rob J Hyndman, Earo Wang, and Nikolay Laptev. Large-scale unusual time series detection. In *2015 IEEE international conference on data mining workshop (ICDMW)*, pp. 1616–1619. IEEE, 2015.

Rob J Hyndman, George Athanasopoulos, Azul Garza, Cristian Challu, Max Mergenthaler, and Kin G. Olivares. *Forecasting: Principles and Practice, the Pythonic Way*. OTexts, Melbourne, Australia, 2025. available at <https://otexts.com/fpppy/>.

Rouba Ibrahim and Pierre L’Ecuyer. Modeling and forecasting call center arrivals: A literature review and a case study. *International Journal of Forecasting*, 32(3):865–874, 2016.

Norman L. Johnson, Samuel Kotz, and N. Balakrishnan. *Continuous Univariate Distributions, Volume 1*. Wiley Series in Probability and Mathematical Statistics. John Wiley & Sons, New York, 2nd edition, 1994.

Diederik P. Kingma and Jimmy Ba. Adam: A method for stochastic optimization, 2015.

Kseniia Kuvshinova, Olga Tsymboi, Alina Kostromina, Dmitry Simakov, and Elizaveta Kovtun. Towards foundation time series model: To synthesize or not to synthesize? *CoRR*, abs/2403.02534, 2024. URL <https://doi.org/10.48550/arXiv.2403.02534>.

Guokun Lai, Wei-Cheng Chang, Yiming Yang, and Hanxiao Liu. Modeling long-and short-term temporal patterns with deep neural networks. In *The 41st international ACM SIGIR conference on research & development in information retrieval*, pp. 95–104, 2018.

Yuxuan Liang, Haomin Wen, Yuqi Nie, Yushan Jiang, Ming Jin, Dongjin Song, Shirui Pan, and Qingsong Wen. Foundation models for time series analysis: A tutorial and survey. In *Proceedings of the 30th ACM SIGKDD Conference on Knowledge Discovery and Data Mining*, pp. 6555–6565, 2024.

Bryan Lim, Sercan Ö. Arik, Nicolas Loeff, and Tomas Pfister. Temporal fusion transformers for interpretable multi-horizon time series forecasting. *International Journal of Forecasting*, 37(4):1748–1764, 2021.

S. Makridakis, A. Andersen, R. Carbone, R. Fildes, M. Hibon, R. Lewandowski, J. Newton, E. Parzen, and R. Winkler. The accuracy of extrapolation (time series) methods: Results of a forecasting competition. *Journal of Forecasting*, 1(2):111–153, 1982.

Spyros Makridakis and Michèle Hibon. The M3-competition: results, conclusions and implications. *International Journal of Forecasting*, 16(4):451–476, 2000. URL <https://www.sciencedirect.com/science/article/pii/S0169207000000571>. The M3- Competition.

Spyros Makridakis, Evangelos Spiliotis, and Vassilios Assimakopoulos. The M4 competition: 100,000 time series and 61 forecasting methods. *International Journal of Forecasting*, 36(1):54–74, 2020. URL <https://www.sciencedirect.com/science/article/pii/S0169207019301128>. M4 Competition.

Paolo Mancuso, Veronica Piccialli, and Antonio Maria Sudoso. A machine learning approach for forecasting hierarchical time series. *Expert Systems with Applications*, 182:115102, 2021. doi: 10.1016/j.eswa.2021.115102.

Luis Moreira-Matias, João Gama, Michel Ferreira, João Mendes-Moreira, and Luís Damas. Predicting taxi-passenger demand using streaming data. *IEEE Transactions on Intelligent Transportation Systems*, 14(3):1393–1402, 2013.

Ashwin Narayan, Bonnie Berger, and Hyunghoon Cho. Density-preserving data visualization unveils dynamic patterns of single-cell transcriptomic variability. *bioRxiv*, pp. 2020–05, 2020.

Yuqi Nie, Nam H. Nguyen, Phanwadee Sinthong, and Jayant Kalagnanam. A time series is worth 64 words: Long-term forecasting with transformers. In *International Conference on Learning Representations*, 2023.

Boris N. Oreshkin, Dmitri Carpov, Nicolas Chapados, and Yoshua Bengio. N-BEATS: neural basis expansion analysis for interpretable time series forecasting. In *8th International Conference on Learning Representations, ICLR 2020*, 2020. URL <https://openreview.net/forum?id=r1ecqn4YwB>.

Boris N Oreshkin, Dmitri Carpov, Nicolas Chapados, and Yoshua Bengio. Meta-learning framework with applications to zero-shot time-series forecasting. In *Proceedings of the AAAI Conference on Artificial Intelligence*, pp. 9242–9250, 2021.

Santosh Palaskar, K Ekambaram, Prasanna Balaprakash, Vikram Ramanarayanan, Narayan Rangaraj, and Nandyala Hemachandra. Automixer for improved multivariate time-series forecasting on business and it observability data. In *Proceedings of the AAAI Conference on Artificial Intelligence*, volume 38, pp. 2840–2848. AAAI Press, 2024. doi: 10.1609/aaai.v38i3.30336.

Adam Paszke, Sam Gross, Francisco Massa, Adam Lerer, James Bradbury, Gregory Chanan, Trevor Killeen, Zeming Lin, Natalia Gimelshein, Luca Antiga, Alban Desmaison, Andreas Kopf, Edward Yang, Zachary DeVito, Martin Raison, Alykhan Tejani, Sasank Chilamkurthy, Benoit Steiner, Lu Fang, Junjie Bai, and Soumith Chintala. Pytorch: An imperative style, high-performance deep learning library. In H. Wallach, H. Larochelle, A. Beygelzimer, F. d’Alché Buc, E. Fox, and R. Garnett (eds.), *Advances in Neural Information Processing Systems*, volume 32, pp. 8024–8035. Curran Associates, Inc., 2019.

Kashif Rasul, Arjun Ashok, Andrew Robert Williams, Hena Ghonia, Rishika Bhagwatkar, Arian Khorasani, Mohammad Javad Darvishi Bayazi, George Adamopoulos, Roland Riachi, Nadhir Hassen, Marin Biloš, Sahil Garg, Anderson Schneider, Nicolas Chapados, Alexandre Drouin, Valentina Zantedeschi, Yuriy Nevmyvaka, and Irina Rish. Lag-Llama: Towards Foundation Models for Probabilistic Time Series Forecasting, 2024.

David Salinas, Valentin Flunkert, Jan Gasthaus, and Tim Januschowski. Deepar: Probabilistic forecasting with autoregressive recurrent networks. *International Journal of Forecasting*, 36(3):1181–1191, 2020.

Artemios-Anargyros Semenoglou, Evangelos Spiliotis, Spyros Makridakis, and Vassilios Assimakopoulos. Investigating the accuracy of cross-learning time series forecasting methods. *International Journal of Forecasting*, 37(3):1072–1084, 2021.

Slawek Smyl. A hybrid method of exponential smoothing and recurrent neural networks for time series forecasting. *International Journal of Forecasting*, 07 2019.

Stephen D. Strowes. Diurnal and weekly cycles in IPv6 traffic. arXiv preprint arXiv:1607.05183, 2016. URL <https://arxiv.org/abs/1607.05183>.

Aris A. Syntetos and John E. Boylan. The accuracy of intermittent demand estimates. *International Journal of Forecasting*, 21(2):303–314, 2005.

M Syntetos, John Boylan, and JD Croston. On the categorization of demand patterns. *Journal of the Operational Research Society*, 56, 05 2005. doi: 10.1057/palgrave.jors.2601841.

Ege Onur Taga, Muhammed Emrullah Ildiz, and Samet Oymak. Timepfn: Effective multivariate time series forecasting with synthetic data. In *Proceedings of the AAAI Conference on Artificial Intelligence*, volume 39, pp. 20761–20769, 2025.

Hugo Touvron, Thibaut Lavril, Gautier Izacard, Xavier Martinet, Marie-Anne Lachaux, Timothée Lacroix, Baptiste Rozière, Naman Goyal, Eric Hambro, Faisal Azhar, Aurélien Rodriguez, Armand Joulin, Édouard Grave, and Guillaume Lample. Llama: Open and efficient foundation language models. *arXiv preprint arXiv:2302.13971*, 2023. URL <https://arxiv.org/abs/2302.13971>.

Artur Trindade. ElectricityLoadDiagrams20112014 dataset. UCI Machine Learning Repository, 2015. URL <https://archive.ics.uci.edu/ml/datasets/electricityloaddiagrams20112014>.

Vivek Vaidya and Jaideep Vaidya. Impact of dimensionality reduction on outlier detection: An empirical study. In *2022 IEEE 4th International Conference on Trust, Privacy and Security in Intelligent Systems, and Applications (TPS-ISA)*, pp. 150–159. IEEE, 2022.

Jingyuan Wang, Jiawei Jiang, Wenjun Jiang, Chengkai Han, and Wayne Xin Zhao. Libcity: A unified library towards efficient and comprehensive urban spatial-temporal prediction, 2023.

Jason Wei, Maarten Bosma, Vincent Y. Zhao, Kelvin Guu, Adams Wei Yu, Brian Lester, Nan Du, Andrew M. Dai, and Quoc V. Le. Finetuned language models are zero-shot learners. In *International Conference on Learning Representations (ICLR)*, April 2022. URL <https://openreview.net/forum?id=gEZrGCozdqR>. Virtual Event.

Ruofeng Wen, Kari Torkkola, Balakrishnan Narayanaswamy, and Dhruv Madeka. A Multi-horizon Quantile Recurrent Forecaster. In *31st Conference on Neural Information Processing Systems NIPS 2017, Time Series Workshop*, 2017. URL <https://arxiv.org/abs/1711.11053>.

Daniel S. Wilks. Intermittent precipitation and its simulation by conditional weather generators. *Agricultural and Forest Meteorology*, 93(3):153–169, 1999.

Walter Willinger, Murad S. Taqqu, Robert Sherman, and Daniel V. Wilson. Self-similarity in high-speed packet traffic: Analysis and modeling of ethernet traffic measurements. In *Statistical Science*, volume 10, pp. 67–85. Institute of Mathematical Statistics, 1995.

Gerald Woo, Chenghao Liu, Akshat Kumar, Caiming Xiong, Silvio Savarese, and Doyen Sahoo. Unified training of universal time series forecasting transformers, 2024. URL <https://arxiv.org/abs/2402.02592>.

Haixu Wu, Jiehui Xu, Jianmin Wang, and Mingsheng Long. Autoformer: Decomposition transformers with auto-correlation for long-term series forecasting. In *NeurIPS*, pp. 101–112, 2021.

Yao-Yuan Yang, Moto Hira, Zhaoheng Ni, Anjali Chourdia, Artyom Astafurov, Caroline Chen, Ching-Feng Yeh, Christian Puhrsich, David Pollack, Dmitriy Genzel, Donny Greenberg, Edward Z. Yang, Jason Lian, Jay Mahadeokar, Jeff Hwang, Ji Chen, Peter Goldsborough, Prabhat Roy, Sean Narenthiran, Shinji Watanabe, Soumith Chintala, Vincent Quenneville-Bélair, and Yangyang Shi. Torchaudio: Building blocks for audio and speech processing. *arXiv preprint arXiv:2110.15018*, 2021.

Jason Yosinski, Jeff Clune, Yoshua Bengio, and Hod Lipson. How transferable are features in deep neural networks?, 2014.

Annan Yu, Danielle C. Maddix, Boran Han, Xiyuan Zhang, Abdul Fatir Ansari, Oleksandr Shchur, Christos Faloutsos, Andrew Gordon Wilson, Michael W. Mahoney, and Yuyang Wang. Understanding the implicit biases of design choices for time series foundation models. *arXiv preprint arXiv:2510.19236*, 2025a.

Annan Yu, Danielle C. Maddix, Boran Han, Xiyuan Zhang, Abdul Fatir Ansari, Oleksandr Shchur, Christos Faloutsos, Andrew Gordon Wilson, Michael W. Mahoney, and Yuyang Wang. Understanding transformers for time series: Rank structure, flow-of-ranks, and compressibility. *arXiv preprint arXiv:2510.03358*, 2025b.

Haoyi Zhou, Shanghang Zhang, Jieqi Peng, Shuai Zhang, Jianxin Li, Hui Xiong, and Wancai Zhang. Informer: Beyond Efficient Transformer for Long Sequence Time-Series Forecasting. *The Association for the Advancement of Artificial Intelligence Conference 2021 (AAAI 2021)*., abs/2012.07436, 2020. URL <https://arxiv.org/abs/2012.07436>.

A GiftEval Benchmark

Table 3: Summary of GiftEval forecasting datasets used in our empirical study.

Dataset	Source	Domain	Frequency	# Series	Avg	Min	Max	# Obs
Jena Weather	Autoformer (Wu et al. 2021)	Nature	10T	1	52,704	52,704	52,704	52,704
Jena Weather	Autoformer (Wu et al. 2021)	Nature	H	1	8,784	8,784	8,784	8,784
Jena Weather	Autoformer (Wu et al. 2021)	Nature	D	1	366	366	366	366
BizITObs - Application	AutoMixer (Palaskar et al. 2024)	Web/CloudOps	10S	1	8,834	8,834	8,834	8,834
BizITObs - Service	AutoMixer (Palaskar et al. 2024)	Web/CloudOps	10S	21	8,835	8,835	8,835	185,535
BizITObs - L2C	AutoMixer (Palaskar et al. 2024)	Web/CloudOps	5T	1	31,968	31,968	31,968	31,968
BizITObs - L2C	AutoMixer (Palaskar et al. 2024)	Web/CloudOps	H	1	2,664	2,664	2,664	2,664
Bitbrains - Fast Storage	Grid Workloads Archive (Shen et al. 2015)	Web/CloudOps	5T	1,250	8,640	8,640	8,640	10,800,000
Bitbrains - Fast Storage	Grid Workloads Archive (Shen et al. 2015)	Web/CloudOps	H	1,250	721	721	721	901,250
Bitbrains - rnd	Grid Workloads Archive (Shen et al. 2015)	Web/CloudOps	5T	500	8,640	8,640	8,640	4,320,000
Bitbrains - rnd	Grid Workloads Archive (Shen et al. 2015)	Web/CloudOps	H	500	720	720	720	360,000
Restaurant	Recruit Rest. Comp. (Howard et al. 2017)	Sales	D	807	358	67	478	289,303
ETT1	Informer (Zhou et al. 2020)	Energy	15T	1	69,680	69,680	69,680	69,680
ETT1	Informer (Zhou et al. 2020)	Energy	H	1	17,420	17,420	17,420	17,420
ETT1	Informer (Zhou et al. 2020)	Energy	D	1	725	725	725	725
ETT1	Informer (Zhou et al. 2020)	Energy	W-THU	1	103	103	103	103
ETT2	Informer (Zhou et al. 2020)	Energy	15T	1	69,680	69,680	69,680	69,680
ETT2	Informer (Zhou et al. 2020)	Energy	H	1	17,420	17,420	17,420	17,420
ETT2	Informer (Zhou et al. 2020)	Energy	D	1	725	725	725	725
ETT2	Informer (Zhou et al. 2020)	Energy	W-THU	1	103	103	103	103
Loop Seattle	LibCity (Wang et al. 2023a)	Transport	5T	323	105,120	105,120	105,120	33,953,760
Loop Seattle	LibCity (Wang et al. 2023a)	Transport	H	323	8,760	8,760	8,760	2,829,480
Loop Seattle	LibCity (Wang et al. 2023a)	Transport	D	323	365	365	365	117,895
SZ-Taxi	LibCity (Wang et al. 2023a)	Transport	15T	156	2,976	2,976	2,976	464,256
SZ-Taxi	LibCity (Wang et al. 2023a)	Transport	H	156	744	744	744	116,064
M_DENSE	LibCity (Wang et al. 2023a)	Transport	H	30	17,520	17,520	17,520	525,600
M_DENSE	LibCity (Wang et al. 2023a)	Transport	D	30	730	730	730	21,900
Solar	LSTNet (Lai et al. 2017)	Energy	10T	137	52,560	52,560	52,560	7,200,720
Solar	LSTNet (Lai et al. 2017)	Energy	H	137	8,760	8,760	8,760	1,200,120
Solar	LSTNet (Lai et al. 2017)	Energy	D	137	365	365	365	50,005
Solar	LSTNet (Lai et al. 2017)	Energy	W-FRI	137	52	52	52	7,124
Hierarchical Sales	Mancuso et al. (2020)	Sales	D	118	1,825	1,825	1,825	215,350
Hierarchical Sales	Mancuso et al. (2020)	Sales	W-WED	118	260	260	260	30,680
M4 Yearly	Monash (Godahewa et al. 2021)	Econ/Fin	A-DEC	22,974	37	19	284	845,109
M4 Quarterly	Monash (Godahewa et al. 2021)	Econ/Fin	Q-DEC	24,000	100	24	874	2,406,108
M4 Monthly	Monash (Godahewa et al. 2021)	Econ/Fin	M	48,000	234	60	2,812	11,246,411
M4 Weekly	Monash (Godahewa et al. 2021)	Econ/Fin	W-SUN	359	1,035	93	2,610	371,579
M4 Daily	Monash (Godahewa et al. 2021)	Econ/Fin	D	4,227	2,371	107	9,933	10,023,836
M4 Hourly	Monash (Godahewa et al. 2021)	Econ/Fin	H	414	902	748	1,008	373,372
Hospital	Monash (Godahewa et al. 2021)	Healthcare	M	767	84	84	84	64,428
COVID Deaths	Monash (Godahewa et al. 2021)	Healthcare	D	266	212	212	212	56,392
US Births	Monash (Godahewa et al. 2021)	Healthcare	D	1	7,305	7,305	7,305	7,305
US Births	Monash (Godahewa et al. 2021)	Healthcare	W-TUE	1	1,043	1,043	1,043	1,043
US Births	Monash (Godahewa et al. 2021)	Healthcare	M	1	240	240	240	240
Saugeen	Monash (Godahewa et al. 2021)	Nature	D	1	23,741	23,741	23,741	23,741
Saugeen	Monash (Godahewa et al. 2021)	Nature	W-THU	1	3,391	3,391	3,391	3,391
Saugeen	Monash (Godahewa et al. 2021)	Nature	M	1	780	780	780	780
Temperature Rain	Monash (Godahewa et al. 2021)	Nature	D	32,072	725	725	725	780
KDD Cup 2018	Monash (Godahewa et al. 2021)	Nature	H	270	10,898	9,504	10,920	2,942,364
KDD Cup 2018	Monash (Godahewa et al. 2021)	Nature	D	270	455	396	455	122,791
Car Parts	Monash (Godahewa et al. 2021)	Sales	M	2,674	51	51	51	136,374
Electricity	UCI ML Archive (Trindade 2015)	Energy	15T	370	140,256	140,256	140,256	51,894,720
Electricity	UCI ML Archive (Trindade 2015)	Energy	H	370	35,064	35,064	35,064	12,973,680
Electricity	UCI ML Archive (Trindade 2015)	Energy	D	370	1,461	1,461	1,461	540,570
Electricity	UCI ML Archive (Trindade 2015)	Energy	W-FRI	370	208	208	208	76,960

In this section, we discuss details of the evaluation GiftEval datasets. The benchmark incorporates data from ten sources, beginning with the Jena Weather dataset, from the Autoformer (Wu et al., 2021). Business and IT observability data from BizITObs (processed via AutoMixer’s pipeline) includes Application, Service, and L2C metrics that combine business KPIs with IT event data (Palaskar et al., 2024). This is complemented by cloud workload data from Bitbrains via the Grid Workloads Archiv (Howard et al., 2017). For energy-related applications, we incorporate electricity transformer temperature datasets (ETT1 and ETT2) from Informer (Zhou et al., 2020), crucial for long-term power deployment monitoring; and urban transportation time series come from LibCity (Wang et al., 2023). Solar plant energy output predictions are sourced from LSTNet (Lai et al., 2018), and sales forecasting data are from Mancuso et al. (2021). We also include a carefully curated subset of the Monash time series collection, selected to avoid overlap with pretraining data (Godahewa et al., 2021), and electricity consumption patterns of 370 clients from the UCI ML Archive (Trindade, 2015). Table 3 provides detailed statistics for each dataset, including source information, frequency, prediction length, number of variates, series length, and total observations.

B M-Series Benchmark

Table 4: Summary of M-series forecasting datasets used in our empirical study.

	Frequency	Seasonality	Horizon	Series	Min Length	Max Length	% Erratic
M1	Monthly	12	18	617	48	150	0
	Quarterly	4	8	203	18	114	0
	Yearly	1	6	181	15	58	0
M3	Other	4	8	174	71	104	0
	Monthly	12	18	1428	66	144	2
	Quarterly	4	8	756	24	72	1
	Yearly	1	6	645	20	47	10
M4	Hourly	24	48	414	748	1008	17
	Daily	1	14	4,227	107	9933	2
	Weekly	1	13	359	93	2610	16
	Monthly	12	18	48,000	60	2812	6
	Quarterly	4	8	24,000	24	874	11
	Yearly	1	6	23,000	19	841	18
Tourism	Monthly	12	24	366	91	333	51
	Quarterly	4	8	427	30	130	39
	Yearly	1	4	518	11	47	23

In this section, we discuss details of the M-series data.

B.1 M1 Dataset Details

The M1 competition (Makridakis et al., 1982) analyzed 1,001 demographic, industrial, and economic time series of varying frequencies and lengths (9-132 observations). The competition revealed that simple methods like ETS (Holt, 1957) often outperformed complex ones, establishing a legacy emphasizing accuracy, automation, and parsimony in forecasting practice.

B.2 M3 Dataset Details

The M3 competition (Makridakis & Hibon, 2000), held 20 years after M1, analyzed 3,003 time series from various domains, with 14-126 observations and multiple frequencies. The competition reaffirmed the superiority of simple forecasting methods, with the `Theta` method (Hyndman & Billah, 2003b) emerging as the top performer.

B.3 M4 Dataset Details

The M4 competition marked a substantial increase in both size and diversity, comprising 100,000 time series across six frequencies and multiple domains. The competition introduced prediction interval evaluation and featured 18 percent non-smooth series (Syntetos et al., 2005). Notably, a neural network model - ESRNN(Smyl, 2019) - outperformed traditional methods for the first time, helping popularize cross-learning (Semenoglou et al., 2021) in global models.

B.4 Tourism Dataset Details

The Tourism dataset (Athanasopoulos et al., 2011) was designed to evaluate forecasting methods applied to tourism demand data across multiple temporal frequencies. It comprises 1,311 time series at monthly, quarterly, and yearly frequencies. This competition introduced the Mean Absolute Scaled Error (MASE) as an alternative metric to evaluate scaled point forecasts, alongside the evaluation of forecast intervals. Notably, 36% of the series were classified as erratic or intermittent. Due to this high proportion of irregular data, the `Naïve1` method proved particularly difficult to outperform at the yearly frequency.

C Deviations from the Zero-Shot Setting in Baselines

Table 5: Summary of zero-shot deviations from baselines. Checkmark indicates that a given dataset was used to pretrain a given model.

Dataset	Source	Chronos	TTM-R2	MOIRAI	TimesFM
M1	Monash (Godahewa et al. 2021)	✗	✗	✓	✗
M3	Monash (Godahewa et al. 2021)	✗	✗	✓	✗
M4	Monash (Godahewa et al. 2021)	✓	✗	✓	✓
Tourism	Monash (Godahewa et al. 2021)	✗	✗	✓	✗
Jena Weather	Autoformer (Wu et al. 2021)	✗	✓	✓	✓
BizITObjs	AutoMixer (Palaskar et al. 2024)	✗	✗	✗	✗
Bitbrains	Grid Workloads Archive (Shen et al. 2015)	✗	✗	✗	✗
Restaurant	Recruit Rest. Comp. (Howard et al. 2017)	✗	✗	✗	✗
ETT	Informer (Zhou et al. 2020)	✗	✗	✗	✗
Loop Seattle	LibCity (Wang et al. 2023a)	✗	✓	✓	✗
SZ-Taxi	LibCity (Wang et al. 2023a)	✗	✓	✓	✗
M_Dense	LibCity (Wang et al. 2023a)	✗	✗	✗	✗
Solar	LSTNet (Lai et al. 2017)	✓	✓	✓	✗
Hierarchical Sales	Mancuso et al. (2020)	✗	✓	✓	✗
Hospital	Monash (Godahewa et al. 2021)	✗	✗	✓	✗
COVID Deaths	Monash (Godahewa et al. 2021)	✗	✓	✓	✗
US Births	Monash (Godahewa et al. 2021)	✗	✓	✓	✗
Saugeen	Monash (Godahewa et al. 2021)	✗	✓	✓	✗
Temperature Rain	Monash (Godahewa et al. 2021)	✗	✓	✓	✗
KDD Cup 2018	Monash (Godahewa et al. 2021)	✓	✓	✓	✗
Car Parts	Monash (Godahewa et al. 2021)	✗	✗	✓	✗
Electricity	UCI ML Archive (Trindade 2015)	✓	✗	✗	✓

In this section, we examine in detail how the baselines reported in Table 1 deviate from a strict zero-shot forecasting regime, as defined in Section 4. While several recent models have been described as “foundation forecasting models” many rely directly on the evaluation datasets as training data. As a result, their performance can not be interpreted as that of a foundation forecasting model.

- **Chronos** (Ansari et al., 2024) paper explicitly distinguishes between pre-train only, in-domain, and zero-shot evaluation settings. Unfortunately, several of the datasets they include in their in-domain evaluation regime (Table 3 of their paper) overlap with the GiftEval and the M-series benchmark collections. The datasets include M4, Solar, KDD cup and Electricity.
- **TTM-R2** (Ekambaram et al., 2024) model was introduced in the context of long-horizon forecasting, and not framed as a zero-shot model. More recently, TTM-R2 and its fine-tuned variants have been explicitly adapted to GiftEval through task-specific fine-tuning, which further departs from the zero-shot foundation model definition.¹ The deviations from the zero-shot regime include the long-horizon Weather dataset, Loop Seattle, Taxi, Solar, Hierarchical Sales, and a big subset of the Monash repository in Hospital, COVID deaths, US births, Saugeen, temperature rain and the KDD cup 2018.
- **MOIRAI** (Woo et al., 2024) was introduced alongside the LOTSA dataset collection, which aggregates the entire Monash repository. This includes the training portions of M1, M3, M4, and Tourism datasets. While the authors report zero-shot results on long-horizon collections such as ETT, Electricity, and Weather, these results are confounded by the fact that Traffic (also part of their long-horizon evaluation) is included in LOTSA pre-training. The MOIRAI method is the most affected by deviations from zero-shot, as they pretrain using 76% of the evaluation datasets.
- **TimesFM** (Das et al., 2024) pre-trains on the full M4 dataset, as well as Electricity, Traffic, and Weather from the long-horizon benchmark suite. Consequently, its reported results on these datasets

¹While not yet published, the TTM-R2 pre-train datasets are mentioned here.

should not be interpreted as zero-shot. At the time of this publication, the `TimesFM` model is the least affected by deviations from the zero-shot regime, using only M4 and Weather.

D Metric Definitions

In this section, we describe several metrics used in our evaluation.

To ensure the comparability of our work with the existing literature, we evaluate the accuracy of the forecasts using *scaled Continuous Ranked Probability Score* (sCRPS, (Gneiting & Raftery, 2007)), defined as:

$$\text{sCRPS}(\mathbf{y}, \hat{\mathbf{Y}}) = \frac{\sum_{i,t,h} \text{CRPS}(y_{i,t,h}, \hat{Y}_{i,t,h})}{\sum_{i,t,h} |y_{i,t,h}|}. \quad (10)$$

That is, the sCRPS is a scaled version of the CRPS in which we divide by the sum of the absolute values of the series. We use a Riemann integral approximation technique that uniformly averages the quantile loss over a discrete set of quantiles:

$$\text{CRPS}(y, \hat{Y}) = 2 \int \rho_\tau(y - F_{\hat{Y}}^{-1}(\tau)) d\tau. \quad (11)$$

We complement the evaluation of the probabilistic forecasts through the *Mean Absolute Scaled Error* (MASE, (Hyndman & Koehler, 2006)), that considers the ratio between mean absolute error of forecasts over mean absolute error of the `SeasonalNaive` forecast $\tilde{y}_{i,t,h}$ (*i.e.*, a point forecast using the last observation on the previous season), defined as:

$$\text{MASE}(\mathbf{y}, \hat{\mathbf{y}}) = \frac{\sum_{i,t,h} |y_{i,t,h} - \hat{y}_{i,t,h}|}{\sum_{i,t,h} |y_{i,t,h} - \tilde{y}_{i,t,h}|}. \quad (12)$$

E Training Methodology and Hyperparameter Settings

In this section, we describe in more detail our training methodology and hyperparameter settings.

E.1 Training Methodology

We train the following zero-shot models on our proposed simulator. We consider **NBEATS**, **MLP** (basically a single block of **NBEATS**), and **PatchTST**. These models represent very different classes of models based on distinct inductive biases (fully-connected design vs. attention-based patching design). Moreover, these are time-tested and generally accepted as strong baselines in forecasting literature. Models are implemented in PyTorch Paszke et al. (2019) using pytorch lightning framework Falcon & The PyTorch Lightning team (2019) trained for 250K (**NBEATS**) and 500K (**PatchTST**) steps using the Adam optimizer Kingma & Ba (2015) with default settings and learning rate 0.0001. Batch size is fixed at 4096 and the model takes the history of 4096 points (the maximum history length reported in the literature) and predicts 512 horizons ahead in one shot. **NBEATS** is trained on 8xV100 machine, and training takes about 16 hours. **PatchTST** is trained on 8xA100 machine, and training takes about 48 hours.

Trained models are applied at inference time with no tuning of parameters or hyperparameters on test datasets. Hyperparameter settings of the neural networks are provided in Tables 6 and 7. Hyperparameter settings of the proposed **SarSim0** simulator are provided in Table 9.

To train the networks, we take the simulator generated sequence of length 6000 samples and randomly choose start and end points of the training sequence of total length 4096 (history) plus 512 (forecast length). We then supply history sequence to the neural network and compute the multi-horizon multi-quantile loss (1) against the forecast ground truth, learning with backpropagation. In order to train the networks to deal with variable sequence length, the 4096-length window is zeroed out on the left with padding mask to simulated the effects of padding (the length of zeroed segment is sampled uniformly from Uniform[0, 4088]). At inference time, short sequences are left padded to length 4096. The output of the network is cut to match the required prediction length (specified by the target dataset). For datasets in GiftEval requiring output lengths longer than 512, we downsample the input by a factor of 2 and upsampled the forecast by the same factor (resulting in output length 1024, which is then trimmed to required forecast length). Downsampling and upsampling are implemented using Kaiser window with filter length 3, rolloff 0.9 from torchaudio Resample function (Yang et al., 2021).

E.2 Hyperparameter Settings

Hyperparameter settings for various models are given in the following tables.

Table 6: **NBEATS** Hyperparameter Settings

Hyperparameter	Value
Batch Size	4096
Learning rate	0.0001
Training steps	250,000
Input length	4096
Ouput length	512
Main Activation Function	ReLU
Number of Blocks	10
Layers within block	3
Block hidden size	1024

Table 7: PatchTST Hyperparameter Settings

Hyperparameter	Value
Batch Size	4096
Learning rate	0.0001
Training steps	500,000
Input Length	4096
Output Length	512
Main Activation Function	ReLU
Patch Length	64
Patch Stride	32
Number of Layers	12
Number of Attention Heads	8
d_model	512
FFN hidden_size	2048
Apply Revin	True
Residualized Attention	True

Table 8: Chronos-Small Hyperparameter Settings

Hyperparameter	Value
Batch Size	1024
Learning rate	0.0001
Training steps	500,000
Input Length	512
Output Length	512
Main Activation Function	ReLU
Patch Length	1
Patch Stride	1
Number of Encoder Layers	6
Number of Decoder Layers	6
Number of Attention Heads	8
use_reg_token	True
d_model	512
d_ff	2048
d_kv	64
Dropout	0

Table 9: **SarSim0** Hyperparameter Settings

Hyperparameter	Value
History Sequence Length	4096
Padding Length	Uniform[0, 4088]
Forecasting Horizon	512
SARIMA Sampling Configuration	
Base Sequence Length	6000
Vectorization Batch Size	256
p , (AR order)	Uniform[0, 10]
q , (MA order)	Uniform[0, 3]
P , (Seasonal AR order)	Uniform[0, 2]
Q , (Seasonal MA order)	Uniform[0, 2]
s , (Seasonality period)	Uniform[0, 52]
r_{\max} (AR max pole radius)	0.9
AR pole angle	Uniform[0, 2π]
R_{\max} (Seasonal AR max pole radius)	0.1
Seasonal AR pole angle	Uniform[0, 2π]
d (Non-seasonal integration order)	Uniform[0, 1]
D (Seasonal integration order)	1
SARIMA-2 Sampling Configuration	
Seasonality pairs	Uniform[[24, 7], [7, 52], [0, 7], [0, 3], [0, 24], [0, 52]]
ϱ (Modulation depth)	Uniform[0, 1]
Additive vs. Multiplicative mixing selection probability	0.5
Noisers Sampling Configuration	
Input selection probability (SARIMA vs. SARIMA-2)	0.5
Noiser selection	Uniform[Poisson, Gamma, Lognormal, Passthrough]
λ_0^P (Base rate for Poisson)	LogUniform[0.1, 100]
λ_0^G (Base rate for Generalized Gamma)	LogUniform[0.1, 100]
λ_0^L (Base rate for Lognormal)	LogUniform[0.1, 5]
κ^P (Shape for Poisson)	N/A
κ^G (Shape for Generalized Gamma)	LogUniform[1, 50.0]
κ^L (Shape for Lognormal)	LogUniform[1, 3.0]
ζ (Power for Generalized Gamma)	Uniform[0.5, 1.5]

E.3 SarSim0 hyperparameter values and selection methodology

The settings of **SarSim0** simulator parameters appear in Table 9, and the detailed explanation for each setting is provided below.

Vectorization Batch Size is set to 256 for on-the-fly generation efficiency.

Model orders p , q , P , Q are set to values often encountered in practice, *e.g.*, 0, 1, 2, 3, with the exception of p , maximum AR order, set to 10, mostly to demonstrate the efficiency of simulator even with higher-order models that are typically more compute hungry. Smaller settings of this parameter yield similar results.

The seasonality period parameter, s , was chosen to cover the typical seasonalities encountered in the data: yearly data typically have seasonality 0 (no seasonality), monthly data often exhibit seasonality 12, quarterly - 4, hourly - 24, weekly - 52, daily - 7. Overall, in order to avoid any benchmark specific biases, we decided to sample seasonalities in SARIMA uniformly in the range covering most common seasonalities: [0, 52].

Similarly, SARIMA-2 was added using the prior knowledge that many practical time series have double seasonalities, with specific motivating examples from the literature laid out at the beginning of Section 4.2. Hourly data with double seasonality often have 24×7 pattern (within day and within week daily patterns); daily data often have 7×52 pattern (within week and within year weekly patterns). Additionally, mixing the seasonality 0 process with the typical natural frequencies listed above, in SARIMA-2, enriches the data with the traces that imitate stochastic-volatility patterns through non-linear cross-modulation. These motivate the choice of SARIMA-2 seasonality pairs, uniformly sampled from this set: [24, 7], [7, 52], [0, 7], [0, 4], [0, 24], [0, 52].

Next, AR max pole radius is chosen to be 0.9 to avoid any numerical issues due to near-unit-root instability that may arise in AR process due to floating quantization error accumulation effects. Similarly, Seasonal AR max pole radius is set to 0.1 for the same reason. Recall that with seasonality $s = 24$ the seasonality pole will be $0.1^{1/24} = 0.89$, for example. AR pole angles are sampled uniformly in $[0, 2\pi]$ - *non-informative prior*.

Non-seasonal integration order is sampled uniformly in $[0, 1]$ - *non-informative prior*.

Seasonal integration order is set to 1. We have tried higher integration orders for both, but they didn't work well because of numerical stability issues in long sequences, so we limit the maximum integration order to 1.

SARIMA-2 Modulation depth is sampled uniformly in $[0, 1]$ - *non-informative prior*.

Additive vs. Multiplicative mixing selection probability is set to 0.5 - *non-informative prior*.

Input selection probability (SARIMA vs. SARIMA-2) is set to 0.5 - *non-informative prior*.

Noiser selection is motivated by the review of relevant literature at the beginning of Section 4.3, documenting the heteroscedasticity, intermittency, and heavy-tailed disturbance effects in real data from multiple unrelated application domains. Poisson, LogNormal and Generalized Gamma processes seem to be the dominating and heavy-tail distribution families that cover a variety of real data. This is why those were chosen, along with a pass-through (no noise) noiser instance. This list is, of course, non-exhaustive, and we believe multiple other noise models are viable and should be explored in future work. The sampling of noisers follows a *non-informative uniform prior*.

Base rate for Poisson is sampled from LogUniform[0.1, 100] for the following reason. First, for large values of rate $\lambda > 100$ Poisson is largely indistinguishable from Gaussian. Second, for very low rate values the Poisson noise produces mostly zeros; for example, with $\lambda = 0.1$, only roughly 1 in 10 samples is non-zero and we decided not to go beyond that. LogUniform distribution is used for rate sampling to concentrate more significant Poisson Noiser mass in a significantly non-Gaussian region of the rates.

Base rate for Generalized Gamma is sampled from LogUniform[0.1, 100], inheriting the range from Poisson.

Base rate for Lognormal is sampled from LogUniform[0.1, 5], where the upper bound is adjusted to 5 to avoid numerical issues. The mean of Log-Normal process is $\exp(\lambda + \sigma^2/2)$, which explodes quickly if either λ or σ are larger than 5-10. The shape of Generalized Gamma is sampled from LogUniform[1, 50.0]. The upper bound is set to 50 as the distribution converges to Gaussian for large shape. Alternatively shape below 1, Gamma density blows up near 0, producing a lot of very small positive values, clustered very close to 0, and a long right tail (cf. the Poisson low-rate zero-dominated case). Shape for Lognormal is sampled from LogUniform[1, 3.0], where we adjust the upper bound to 3, so that mean of the process is limited by a reasonable number, $\exp(5 + 3^2/2) \approx 13360$, also effects of rate 5 and variance $3^2/2 = 4.5$ are roughly equal; whereas the lower bound corresponds to the LogNormal with unit variance.

Finally, Power for Generalized Gamma is sampled from Uniform[0.5, 1.5] so that $\zeta = 1$ (standard Gamma) sits in the middle, while the interval explores a moderate range of heavier-tailed ($\zeta < 1$) and lighter-tailed ($\zeta > 1$) shapes. For smaller values of ζ , the density again blows up near zero; whereas for larger values we have observed some numerical issues arising from taking a significant power of a large number.

F ForecastPFN and KernelSynth Synthetic Generators

In this section, we provide detailed implementation and analysis of two synthetic time series generators used in recent foundation models: ForecastPFN’s ETS-based generator (Dooley et al., 2023) and Chronos’s KernelSynth GP-based generator (Ansari et al., 2024). Both methods generate diverse training data, but they employ fundamentally different mechanisms—structured multiplicative decomposition versus compositional Gaussian processes. We present their mathematical formulations, our optimized implementations, and empirical comparisons of computational efficiency and scalability.

ForecastPFN ETS Generator. ForecastPFN Dooley et al. (2023) generates synthetic training data using a structured prior based on a multiplicative Error-Trend-Seasonality (ETS) decomposition. Each series is modeled as the product of a trend, a multi-scale seasonal component, and a Weibull-distributed noise factor, with all underlying parameters drawn from prior distributions to create the synthetic training corpus. The formal composition is given by the following: The component periods are set to standard values (e.g., $p_{\text{week}} = 7$, $p_{\text{month}} = 30.5$). Parameters for trend are drawn from Gaussian priors, while Fourier coefficients for seasonality are scaled as $c_{f,\nu}, d_{f,\nu} \sim \mathcal{N}(0, 1/f)$ and normalized to a unit sum-of-squares. Crucially, the model trains on the noise-free targets $\psi(t)$ rather than the full series y_t , accelerating convergence while maintaining generalization to noisy real-world data. Here are the details:

$$\begin{aligned}
y_t &= \psi(t) z_t = \text{trend}(t) \text{seasonal}(t) z_t, \\
z_t &= 1 + m_{\text{noise}} (z - \bar{z}), \quad z \sim \text{Weibull}(1, k), \quad \bar{z} = (\ln 2)^{1/k}, \\
\text{trend}(t) &= (1 + m_{\text{lin}} t + c_{\text{lin}}) (m_{\text{exp}} c_{\text{exp}}^t), \\
\text{seasonal}(t) &= \prod_{\nu \in \{\text{week, month, year}\}} \text{seasonal}_{\nu}(t), \\
\text{seasonal}_{\nu}(t) &= 1 + m_{\nu} \sum_{f=1}^{\lfloor p_{\nu}/2 \rfloor} \left[c_{f,\nu} \sin\left(\frac{2\pi f t}{p_{\nu}}\right) + d_{f,\nu} \cos\left(\frac{2\pi f t}{p_{\nu}}\right) \right], \\
\text{with } p_{\text{week}} &= 7, \quad p_{\text{month}} = 30.5, \quad p_{\text{year}} = 365.25, \quad \sum_f (c_{f,\nu}^2 + d_{f,\nu}^2) = 1.
\end{aligned}$$

We compared the official ForecastPFN implementation against our optimized vectorized implementation using 50,000 synthetic time series samples to ensure mathematical equivalence. All statistical tests (Kolmogorov-Smirnov, Mann-Whitney U) show no significant differences ($p > 0.05$), with negligible effect sizes (Cohen’s $d < 0.01$), confirming statistical equivalence between implementations. Our optimized vectorized implementation achieves $14.6 \times$ average speedup with 86.8% time reduction while maintaining statistical equivalence to the original implementation.

Table 10: Statistical Comparison: Official vs. Our Vectorized Implementation (n=50,000)

Metric	Official $\mu \pm \sigma$	Our Impl. $\mu \pm \sigma$	KS p-value	MW p-value	Cohen’s d
Range	20.56 ± 36.66	20.91 ± 37.97	0.648	0.888	0.009
Mean	0.85 ± 11.14	0.94 ± 11.37	0.579	0.243	0.008
Std Deviation	5.22 ± 9.08	5.29 ± 9.35	0.894	0.871	0.008
Trends	0.006 ± 0.222	0.008 ± 0.227	0.458	0.206	0.009
Seasonality	13.13 ± 3.55	13.14 ± 3.55	0.803	0.724	0.004
Noise Level	2.33 ± 4.30	2.36 ± 4.46	0.336	0.799	0.006

KernelSynth. KernelSynth is a GP-based synthetic time series generator that *inverts* the Automatic Statistician: rather than discovering kernel compositions to explain data, it randomly composes kernels to *produce* diverse temporal patterns (Ansari et al., 2024; Duvenaud et al., 2013). The method maintains a kernel bank \mathcal{K} capturing fundamental patterns—Linear (trends), Periodic (seasonality at daily/weekly/monthly/yearly

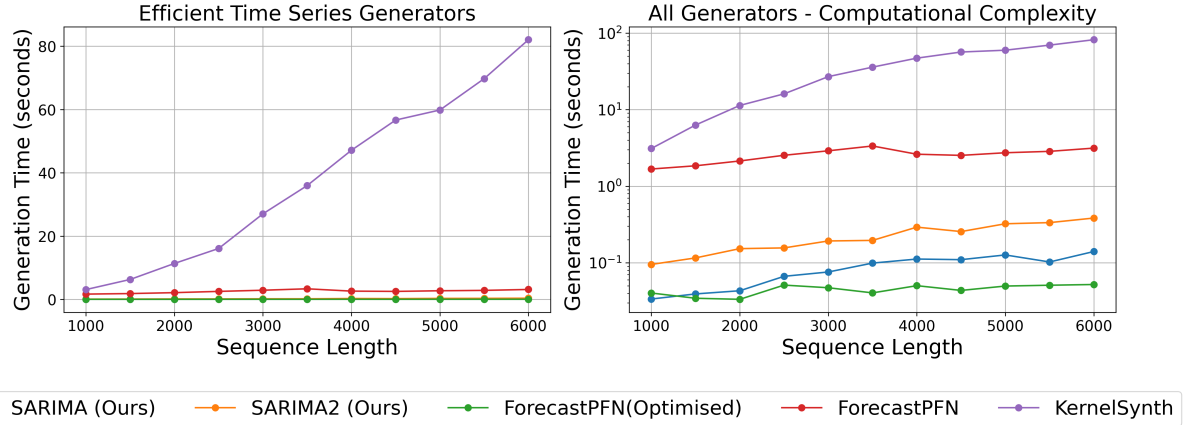


Figure 4: The time per time-series comparison of different simulators.

scales), RBF (smooth local variations), Rational Quadratic (multi-scale structures), Constant (bias), and White Noise (stochastic components). Generation proceeds by sampling $j \sim \mathcal{U}\{1, J\}$ kernels with replacement and hierarchically combining them via random binary operations (+ or \times) into a composite covariance $\tilde{\kappa}(t, t')$, where addition superposes independent patterns and multiplication creates localized interactions (e.g., RBF \times Periodic yields locally periodic patterns that decay). Finally, a length- ℓ_{syn} time series is drawn from the GP prior $\mathcal{GP}(0, \tilde{\kappa})$. We now detail the mathematical formulation of these three core components. The generation pipeline consists of the following elements:

- **Kernel bank \mathcal{K} :** Constant $k_C = \sigma_c^2$; White $k_W = \sigma_n^2 \delta_{t,t'}$; Linear $k_L \propto tt'$; RBF $k_{\text{RBF}} \propto \exp(-\Delta t^2/2\ell^2)$; Rational-Quadratic $k_{\text{RQ}} \propto (1 + \Delta t^2/2\alpha\ell^2)^{-\alpha}$; Periodic $k_{\text{Per}} \propto \exp(-2\sin^2(\pi\Delta t/p)/\ell^2)$ with periods $p \in \{4, 6, 12, 24, 26, 30, 48, 52, 60, 96, 365, 730\}/\text{LENGTH}$.
- **Compositional grammar:** Sample $j \sim \mathcal{U}\{1, J\}$ kernels $\kappa_1, \dots, \kappa_j$ from \mathcal{K} ; fold recursively via random $\star \in \{+, \times\}$ to get $\tilde{\kappa} = (((\kappa_1 \star \kappa_2) \star \kappa_3) \dots)$. Addition superposes independent effects; multiplication localizes/gates patterns.
- **GP sampling:** Grid $t_{1:n}$ ($n = 1024$), build covariance $K_{ij} = \tilde{\kappa}(t_i, t_j)$, draw $\mathbf{x} \sim \mathcal{N}(\mathbf{0}, K)$.

Table 11: Comparison of synthetic time series generation methods

Method	Scales with Length	On-the-fly Synthesis*	Generalization
ForecastPFN	✓	✗	✗
KernelSynth	✗	✗	✗
SarSim0 (ours)	✓	✓	✓

The time per time-series comparison of different simulators is presented in Figure 4. We note that the KernelSynth generation speed is very slow compared to other alternatives. For ForecastPFN we were able to achieve comparable speed via vectorization of the original code.

G UMAP Visualization Analysis

In this section, we provide more details on our visualization analysis.

The UMAP visualization in Figure 3 of the main paper demonstrates a significant and impressive overlap between the synthetic data generated by the SARIMA simulator and the real-world M4-monthly time series. Here, we describe a principled and automated methodology to move beyond visual inspection, systematically identifying and characterizing the real-world patterns that the samples SARIMA simulator do not cover.

G.1 Methodology

To identify these missing patterns, we employ a two-stage pipeline that first learns a low-dimensional representation of the time series, *e.g.*, through UMAP, and then uses a density-based algorithm to score and rank real series based on their novelty with respect to the synthetic distribution.

Dimensionality Reduction with UMAP and DensMAP. To maintain consistency with the main paper, our initial analysis uses Uniform Manifold Approximation and Projection (UMAP). As a complementary approach for a more robust analysis, we also use its density-preserving variant, DensMAP (Narayan et al., 2020). While UMAP is powerful for visualizing cluster structures, its assumption of uniform point distribution on the manifold can distort local density information. DensMAP refines this by adding a density-preservation term to its objective function, producing an embedding that more faithfully represents the local densities of the original data space, which is critical for the subsequent novelty detection step. Our DensMAP results are not presented here to manage the document size, but results were qualitatively similar.

Novelty Detection with Local Outlier Factor (LOF). We use the LOF algorithm (Breunig et al., 2000) for density-based novelty detection. For each embedding method (UMAP and DensMAP), an LOF model is trained exclusively on the embeddings of the synthetic series. This model learns the density patterns of the “normal” data as defined by the SARIMA sampler. Each real series is then scored by this model, where a more negative score indicates that the series lies in a low-density region of the synthetic data manifold and is thus considered novel. The high-level approach of combining dimensionality reduction with outlier detection is a well-established technique for identifying anomalous time series. While our method learns embeddings directly from raw time series, Hyndman et al. (2015) have successfully used feature-based approaches. Furthermore, Vaidya & Vaidya (2022) provides empirical evidence that dimensionality reduction can preserve or even enhance the performance of outlier detection algorithms, supporting the validity of our pipeline.

We use default values for the hyperparameters of the LOF model. Series with lowest 5% novelty score are considered as “novel.”

G.2 Analysis of M4-monthly Series

Novelty Detection with LOF. We apply our novelty detection pipeline to the M4-monthly dataset across four experimental settings, varying both the dimensionality reduction technique (UMAP vs. DensMAP) and the synthetic data source (basic SARIMA vs. the full `SarSim0` simulator). We supplement the analysis on the samples of the full `SarSim0` because they are the actual samples feed into the model during training.

In total there are four sets of experiments, each of which are demonstrated by two figures:

1. Identifying Novel M4-monthly Series with UMAP/DensMAP and LOF. The left panel shows the 2D embedding space, visualizing the coverage of the M4-monthly dataset by synthetic samples. Real-world series are categorized as covered by the synthetic distribution (green), novel (orange), or among the top-200 most novel (red stars). The right panel displays the same M4-monthly embeddings, colored by their LOF novelty score, highlighting that the most novel series (red) form distinct clusters at the edges of the synthetic data distribution.
2. Visualization of the Top 100 Most Novel M4-monthly Series. This figure visualizes the time series corresponding to the 100 lowest LOF novelty scores from the UMAP/DensMAP analysis.

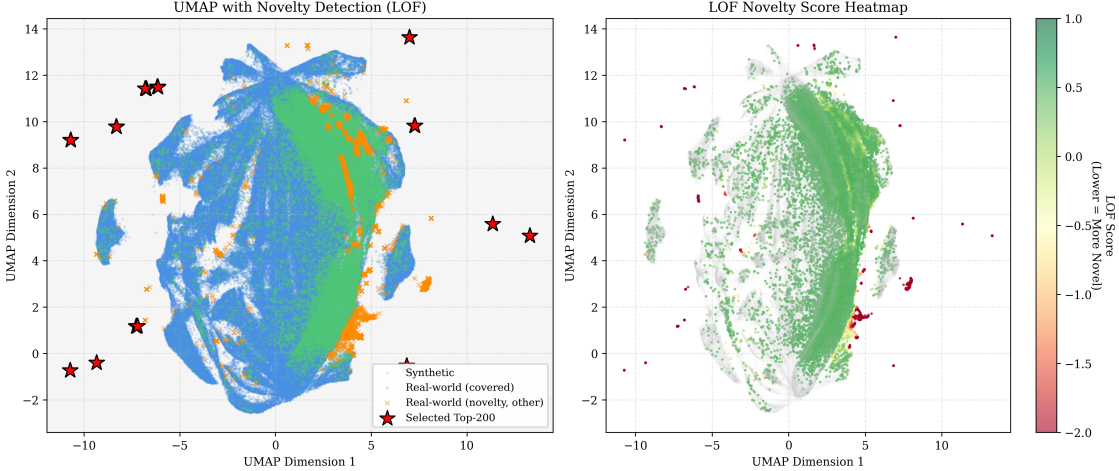


Figure 5: **Baseline SARIMA + M4-monthly + UMAP.** LOF novelty detection results.

SARIMA + UMAP. See Figure 5 and Figure 6.

SarSim0 + UMAP. See Figure 7 and Figure 8.

Our findings can be summarized in two key points:

First, the combination of dimensionality reduction and the LOF algorithm is an effective pipeline for systematically identifying simulator coverage gaps. Across both UMAP and DensMAP embeddings, the LOF novelty scores align with visual inspection: the series that form distinct, uncovered clusters in the embedding space are precisely those that receive the highest novelty scores. This confirms that the “holes” are not mere visualization artifacts, but instead represent statistically significant deviations from the synthetic data distribution.

Second, a consistent and interpretable pattern emerged from the top-ranked novel series across all four experimental settings. These typically correspond to time series windows with: (i) abrupt level shifts or structural breaks (*i.e.*, trend slope change or more generally generating process change); (ii) strong, isolated spikes or outages that do not repeat seasonally (especially isolated aperiodic negative spikes); or (iii) patterns with pronounced quasi-periodic calendar effects that are not captured by purely seasonal-period-based SARIMA specification.



Figure 6: **Baseline SARIMA + M4-monthly + UMAP.** Top 100 novel M4-monthly series visualization

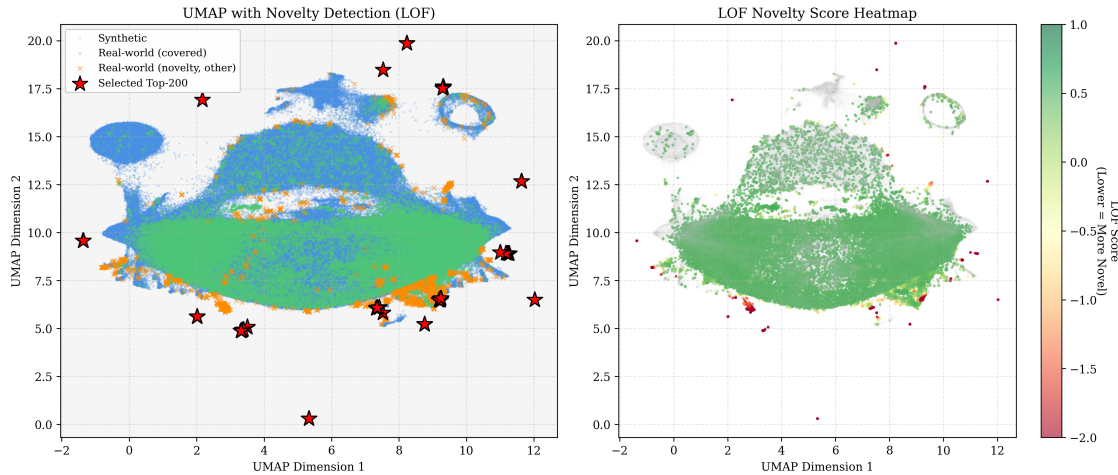


Figure 7: **SarSim0 + M4-monthly + UMAP.** LOF novelty detection results.



Figure 8: SarSim0 + M4-monthly + UMAP. Top 100 novel M4-monthly series visualization

	Duffing		Lorenz		Lotka-Volterra		Pendulum	
	MSE	MAE	MSE	MAE	MSE	MAE	MSE	MAE
Chronos-Large	0.709	0.524	59.2	5.3	2e-4	0.011	0.079	0.174
Chronos-Base	0.671	0.487	57.1	5.1	3e-4	0.011	0.020	0.070
Chronos-Small	0.516	0.432	44.3	4.6	5e-4	0.014	0.150	0.250
Chronos-Mini	0.640	0.548	66.7	6.1	6e-4	0.016	0.849	0.638
Chronos-Tiny	0.798	0.581	57.7	5.5	2e-3	0.026	2.700	1.100
TimesFM	0.718	0.564	77.2	6.1	9e-5	0.006	0.807	0.533
NBEATS-SarSim0	0.609	0.550	56.0	5.7	4e-4	0.014	0.375	0.445
Chronos-SarSim0	0.650	0.510	63.2	5.8	4e-5	0.003	1.220	0.672
PatchTST-SarSim0	0.750	0.550	55.1	5.6	4e-5	0.004	0.294	0.366

Table 12: Zero-shot forecasting performance on four nonlinear dynamical systems (Duffing, Lorenz, Lotka-Volterra, Pendulum), reported as MSE and MAE for each system.

H Additional Results

In this section, we describe additional empirical results based on non-linear dynamical systems.

H.1 Non-linear systems results

To probe the behavior well outside the target regime of traditional statistics based time series, we ran an additional zero-shot experiment on four canonical nonlinear dynamical systems (Duffing, Lorenz, Lotka-Volterra, Pendulum), comparing several **Chronos** variants, **TimesFM**, and **NBEATS**/PatchTST/**Chronos** models trained on **SarSim0**. We generated datasets for the four non-linear dynamical systems. For each dynamical system, we simulated a single long trajectory of 20,000 time steps. The initial 16,000 steps are treated as burn-in, and the final 4,000 steps are used for forecasting evaluation. Evaluation results appear in Table 12, while the data-generation procedure for each system is summarized below.

Across the four canonical nonlinear systems we explored, the error levels of **SarSim0**-pretrained models are generally in the same range as those of the real-data foundation models. We see this as evidence that, on nonlinear dynamical systems far from our intended application domain and including aperiodic/chaotic behavior, pretraining on a SARIMA-based synthetic family still yields models that behave reasonably and on a similar scale to models trained on real data. This suggests that the inductive biases used to construct the simulator are not overly restrictive: while they clearly favour series dominated by trend, seasonality, and intermittency, they remain compatible with the level of out-of-domain generalization observed in real-data-pretrained models.

Pendulum. We consider a nonlinear simple pendulum described by its angular displacement and angular velocity. Each trajectory is initialized with a random starting angle and angular velocity, and then evolved forward in time using the standard equations of motion under gravity. The physical system is a point mass m attached to a massless rigid rod of length l , moving in a vertical plane under constant gravitational acceleration g . The dynamics of the pendulum are governed by the following second-order differential equation:

$$\theta''(t) + \frac{g}{l} \sin(\theta(t)) = 0, \quad (13)$$

where:

- $\theta(t)$ is the angular displacement of the pendulum at time t ,
- $\theta''(t)$ is the angular acceleration,
- g is the acceleration due to gravity (9.81 m/s^2),
- l is the length of the pendulum (set to 1.0 m).

The system is further characterized by its initial conditions:

- the initial angle θ_0 , which is randomly chosen from a uniform distribution between $-\pi$ and π , and
- the initial angular velocity ω_0 , which is randomly chosen from a uniform distribution between -1 rad/s and 1 rad/s.

The motion of the pendulum is modeled using numerical methods, specifically the Euler method, which approximates the solution of the system of equations over discrete time steps.

Duffing Oscillator. We consider a nonlinear oscillator with damping and a cubic restoring term. For each run, we sample random initial displacement and velocity, and we then evolve the system under a periodic external forcing. The underlying dynamics follow the Duffing oscillator, a canonical nonlinear second-order system used to model oscillators with nonlinear stiffness and damping. Its evolution is governed by the differential equation:

$$\ddot{x} + \delta\dot{x} + \alpha x + \beta x^3 = \gamma \cos(\omega t),$$

where $x(t)$ denotes the oscillator's displacement, $y(t) = \dot{x}(t)$ its velocity, and t the time variable. The system parameters are fixed to $\alpha = 1.0$ (linear stiffness), $\beta = 5.0$ (nonlinear stiffness), $\delta = 0.3$ (damping coefficient), $\gamma = 8.0$ (driving force amplitude), and $\omega = 0.5$ (angular frequency of the driving force). The oscillator is subject to a periodic external drive, and its evolution reflects the combined effects of the nonlinear restoring force and damping. We simulate the dynamics by numerically integrating the equations of motion with a simple time-stepping scheme, where dt is the time step and the initial conditions for x and y are drawn at random from a small interval. For this choice of parameters, the resulting motion exhibits chaotic behavior.

Lotka-Volterra. We also include a predator-prey population system, in which prey and predator counts evolve through their mutual interaction. Each trajectory starts from randomly chosen initial population levels, and the dynamics are then propagated forward according to the classical Lotka-Volterra equations. The governing equations for the Lotka-Volterra predator-prey model are given by:

$$\begin{aligned} \frac{dN_{\text{prey}}}{dt} &= \alpha N_{\text{prey}} - \beta N_{\text{prey}} N_{\text{predator}} \\ \frac{dN_{\text{predator}}}{dt} &= \delta N_{\text{prey}} N_{\text{predator}} - \gamma N_{\text{predator}}, \end{aligned}$$

where:

- N_{prey} is the population of the prey species,
- N_{predator} is the population of the predator species,
- α is the natural growth rate of the prey,
- β is the predation rate (rate at which predators kill prey),
- δ is the rate at which predators increase due to consuming prey,
- γ is the natural death rate of the predator.

In this formulation, the prey population grows exponentially when predators are absent, while the predator population decays exponentially if no prey are available. Their interaction leads to characteristic cyclical oscillations in both population sizes.

We simulate the system by numerically integrating the differential equations with a simple Euler scheme. At the start of each run, prey and predator populations are initialized at random within a prescribed interval. The parameters $\alpha = 1.1$, $\beta = 0.4$, $\delta = 0.1$, and $\gamma = 0.4$ are then used to update the populations at every time step.

	GiftEval		M-SERIES	
	sCRPS	MASE	sCRPS	MASE
NBEATS-SarSim0-default	0.602	0.849	0.096	0.869
NBEATS-SarSim0-p=3	0.603	0.851	0.097	0.876
NBEATS-SarSim0-p=7	0.600	0.846	0.096	0.867
NBEATS-SarSim0-p=15	0.599	0.850	0.097	0.869
NBEATS-SarSim0-p=20	0.602	0.852	0.097	0.872
NBEATS-SarSim0- $r_{\max} = 0.8$	0.601	0.848	0.096	0.870
NBEATS-SarSim0- $r_{\max} = 0.95$	0.600	0.847	0.097	0.873
NBEATS-SarSim0- $R_{\max} = 0.2$	0.601	0.844	0.096	0.869
NBEATS-SarSim0- $R_{\max} = 0.5$	0.598	0.846	0.096	0.866
NBEATS-SarSim0-q=6	0.604	0.848	0.097	0.875
NBEATS-SarSim0-Q=4	0.602	0.851	0.097	0.871

Table 13: Study of the sensitivity of **NBEATS-SarSim0** to simulator hyperparameters.

Lorenz '63. We also consider a chaotic dynamical system with three state variables x , y , and z . Each trajectory is initialized from random starting conditions and then evolved forward in time using the Lorenz equations under standard parameter settings. The equations governing the Lorenz system are given by:

$$\frac{dx}{dt} = \sigma(y - x)$$

$$\frac{dy}{dt} = x(\rho - z) - y$$

$$\frac{dz}{dt} = xy - \beta z,$$

where:

- x , y , and z represent the state variables of the system, typically interpreted as the variables describing the convection rolls in the atmosphere,
- σ is the Prandtl number, a measure of the fluid's viscosity, set to 10.0,
- ρ is the Rayleigh number, representing the temperature difference between the top and bottom of the fluid, set to 28.0,
- β is a geometric factor, set to $\frac{8}{3}$.

For this choice of parameters, the Lorenz system displays chaotic dynamics: even tiny perturbations in the initial state can evolve into drastically different trajectories over time. In our experiments, we integrate the system of differential equations using the Euler method over a finite sequence of time steps.

H.2 SarSim0 Hyperparameter Sensitivity Analysis

In our evaluation, we varied several simulator hyperparameters: the maximum AR order p , the AR pole radius bounds r_{\max} and R_{\max} , seasonal and non-seasonal MA orders (q, Q) around the default configuration, retraining **NBEATS-SarSim0** under the same protocol. Results are summarized in Table 13. Across all these variants, performance on both GiftEval and the M-Series remains very similar to the default configuration. This indicates that **SarSim0** is not a brittle “sweet spot”: the configuration we use appears relatively benchmark-agnostic and robust to substantial hyperparameter changes, rather than being reliant on finely tuned settings.

	Econ/Fin	Energy	Healthcare	Nature	Sales	Transport	Web/CloudOps
Chronos-Base	0.798	0.733	0.513	0.451	0.444	0.594	0.824
Chronos-Small	0.810	0.753	0.525	0.472	0.449	0.614	0.797
MOIRAI-Large	0.778	0.732	0.565	0.382	0.445	0.451	0.748
MOIRAI-Small	0.834	0.763	0.744	0.413	0.442	0.551	0.777
TTM-R2-Pretrained	1.316	0.944	1.375	0.506	0.765	0.750	1.055
TimesFM	0.761	0.783	0.690	0.411	0.421	0.591	0.935
NBEATS	1.027	1.088	0.755	0.656	0.507	0.688	0.722
PatchTST	0.854	0.712	0.609	0.428	0.426	0.535	0.553
AutoARIMA	0.873	0.969	0.603	0.811	0.561	0.884	1.144
NBEATS-KernelSynth	0.985	0.827	0.609	0.489	0.517	0.649	0.739
NBEATS-ForecastPFN	3.640	1.459	2.211	0.603	0.462	0.866	1.174
PatchTST-KernelSynth	0.955	0.782	0.586	0.479	0.518	0.605	0.754
PatchTST-ForecastPFN	3.904	1.751	3.029	0.656	0.515	1.141	1.333
NBEATS-SarSim0	0.845	0.718	0.516	0.413	0.420	0.556	0.641
PatchTST-SarSim0	0.821	0.687	0.511	0.380	0.417	0.546	0.596
MLP-SarSim0	0.878	0.745	0.655	0.431	0.425	0.597	0.710

Table 14: nCRPS on GiftEval, weighted aggregation by domain. Lower values are better.

H.3 Detailed GiftEval Results

H.3.1 GiftEval Domain Split

We report GiftEval results stratified by domain in Tables 14-15 (see Table 1 and its discussion for model and baseline details). An important contextual point is that the Econ/Fin subset of GiftEval is essentially the M4 competition data, which we show in Appendix C (Table 5) to be included in the pretraining corpora of **Chronos**, **MOIRAI**, and **TimesFM**. Consequently, on Econ/Fin these foundation models are not in a strict zero-shot regime, whereas **SarSim0**-pretrained backbones never see these series during training and therefore operate under strict zero-shot conditions. Even in this favorable setting for the real-data models, their accuracy advantage on Econ/Fin is relatively modest, with **SarSim0** models trailing only slightly behind. On the remaining six domains (*i.e.*, excluding Econ/Fin), **SarSim0**-trained models provide either very comparable or clearly better accuracy. In terms of sCRPS, a **SarSim0** backbone achieves the best score in 4 out of 6 domains (Energy, Healthcare, Nature, Sales), and is close to the best method on Transport and Web/CloudOps. For nMASE, **SarSim0** is best in 2 out of 6 domains (Sales, Web/CloudOps), and it typically remains within a small margin of the strongest model in the others. Overall, this pattern suggests that the inductive biases of **SarSim0** are not tuned to any single domain, but generalize robustly across diverse application areas.

A second observation from Tables 14-15 is the uniform dominance of **SarSim0** over other synthetic generators. Fixing the backbone (N-BEATS or PatchTST) and varying only the pretraining corpus, **SarSim0** consistently outperforms both KernelSynth and ForecastPFN across all GiftEval domains and for both nCRPS and nMASE. For example, **NBEATS-SarSim0** and **PatchTST-SarSim0** are strictly better than their KernelSynth- and ForecastPFN-pretrained counterparts in Econ/Fin, Energy, Healthcare, Nature, Sales, Transport, and Web/CloudOps.

A third comparison is with the non-zero-shot **NBEATS** and **PatchTST** baselines that are fully supervised on each GiftEval dataset. For **NBEATS**, **SarSim0**-pretrained **NBEATS** strictly improves over dataset-specific **NBEATS** on all seven domains in nCRPS and on 6 of 7 domains in nMASE (the remaining Web/CloudOps gap is negligible), despite never seeing real data during pretraining. For **PatchTST**, **PatchTST-SarSim0** matches or improves upon the supervised **PatchTST** baseline on the majority of domains (5/7 in nCRPS and 6/7 in nMASE), with only Web/CloudOps (and slightly Transport in nCRPS) still favouring in-domain supervised training.

	Econ/Fin	Energy	Healthcare	Nature	Sales	Transport	Web/CloudOps
Chronos-Base	0.783	0.924	0.644	0.823	0.726	0.712	1.140
Chronos-Small	0.797	0.948	0.607	0.852	0.733	0.737	1.144
MOIRAI-Large	0.845	1.026	0.699	0.750	0.711	0.601	1.125
MOIRAI-Small	0.985	1.069	0.848	0.807	0.731	0.731	1.136
TTM-R2-Pretrained	1.409	1.016	1.176	0.851	0.977	0.792	1.254
TimesFM	0.824	1.017	0.698	0.880	0.701	0.741	2.394
NBEATS	0.861	1.185	0.690	0.933	0.705	0.730	0.916
PatchTST	0.907	0.983	0.685	0.916	0.691	0.709	0.780
AutoARIMA	0.866	1.011	0.783	1.018	0.813	0.973	1.615
NBEATS-KernelSynth	1.013	1.131	0.705	0.975	0.803	0.846	1.033
NBEATS-ForecastPFN	6.009	2.066	2.229	1.134	0.769	1.165	1.688
PatchTST-KernelSynth	1.020	1.072	0.699	0.936	0.805	0.793	1.012
PatchTST-ForecastPFN	6.266	1.993	2.744	1.110	0.821	1.338	1.919
NBEATS-SarSim0	0.830	0.965	0.620	0.817	0.688	0.718	0.918
PatchTST-SarSim0	0.844	0.945	0.665	0.797	0.690	0.708	0.891
MLP-SarSim0	0.985	1.004	0.777	0.858	0.695	0.767	0.976

Table 15: nMASE on GiftEval, weighted aggregation by domain. Lower values are better.

frequency	10S	10T	15T	5T	A	D	H	M	Q	W
Chronos-Base	1.442	0.546	0.833	0.712	0.984	0.476	0.562	0.854	0.850	0.621
Chronos-Small	1.331	0.629	0.859	0.711	1.014	0.500	0.569	0.823	0.856	0.614
MOIRAI-Large	1.464	0.566	0.809	0.480	0.758	0.473	0.497	0.786	0.749	0.726
MOIRAI-Small	1.638	0.590	0.809	0.551	0.766	0.483	0.552	0.985	0.803	0.788
TTM-R2-Pretrained	2.255	0.511	0.951	0.755	1.436	0.789	0.688	1.495	1.416	1.354
TimesFM	2.177	0.528	0.853	0.701	0.853	0.520	0.570	0.737	0.863	0.689
NBEATS	1.003	0.791	1.070	0.728	0.977	0.660	0.730	0.968	0.983	1.112
PatchTST	0.899	0.498	0.729	0.544	0.853	0.494	0.495	0.837	0.844	0.763
AutoARIMA	1.678	1.149	1.059	1.042	0.948	0.590	0.903	0.764	0.832	0.837
NBEATS-KernelSynth	1.149	0.545	0.823	0.674	1.259	0.556	0.658	0.829	0.950	0.761
NBEATS-ForecastPFN	2.142	0.823	1.425	1.001	2.940	0.909	1.013	1.518	3.061	1.500
PatchTST-KernelSynth	1.151	0.504	0.797	0.688	1.272	0.554	0.604	0.825	0.957	0.784
PatchTST-ForecastPFN	3.349	1.017	1.537	1.112	3.171	0.968	1.154	2.191	2.716	2.276
NBEATS-SarSim0	1.153	0.501	0.718	0.576	0.963	0.470	0.546	0.713	0.827	0.649
PatchTST-SarSim0	1.114	0.440	0.702	0.530	0.998	0.455	0.507	0.755	0.821	0.656
MLP-SarSim0	1.408	0.534	0.743	0.616	1.211	0.482	0.570	0.840	0.912	0.716

Table 16: nCRPS on GiftEval, weighted aggregation by frequency. Lower values are better.

Overall, this stratified view shows that much of the benefit usually attributed to per-dataset supervised training can instead be recovered from a single, domain-agnostic `SarSim0` curriculum, with only a narrow slice of domains where additional task-specific fitting still offers an advantage.

H.3.2 GiftEval Frequency Split

We further stratify GiftEval by sampling frequency in Tables 16-17. As detailed in Appendix C, the pretraining corpora of `Chronos`, `MOIRAI`, `TimesFM`, and `TTM` include large portions of the M4 competition data, whose dominant frequencies are annual (A), quarterly (Q), and monthly (M). In fact, the Annual and Quarterly splits in GiftEval consist exclusively of M4-yearly and M4-quarterly, respectively. The Monthly split aggregates five

	10S	10T	15T	5T	A	D	H	M	Q	W
Chronos-Base	2.481	1.088	0.887	0.862	0.918	0.714	0.791	0.857	0.768	0.762
Chronos-Small	2.479	1.204	0.919	0.872	0.943	0.737	0.802	0.827	0.774	0.746
MOIRAI-Large	2.486	1.125	0.984	0.672	0.749	0.727	0.792	0.825	0.712	0.931
MOIRAI-Small	2.419	1.161	0.986	0.773	0.751	0.752	0.899	1.016	0.774	0.968
TTM-R2-Pretrained	2.933	0.917	0.905	0.863	1.294	0.981	0.883	1.207	1.265	1.225
TimesFM	3.733	1.274	0.956	2.380	0.845	0.746	0.855	0.800	0.874	0.847
NBEATS	1.284	1.213	1.016	0.884	0.794	0.775	0.905	0.851	0.755	1.083
PatchTST	1.063	1.189	0.877	0.786	0.830	0.749	0.803	0.859	0.824	0.929
AutoARIMA	4.744	1.001	0.978	1.000	0.935	0.882	1.060	0.759	0.799	0.947
NBEATS-KernelSynth	1.784	1.146	0.958	0.874	1.268	0.888	1.003	0.846	0.923	0.924
NBEATS-ForecastPFN	3.844	1.794	1.765	1.261	3.317	1.317	1.648	1.685	3.996	2.011
PatchTST-KernelSynth	1.760	1.103	0.939	0.858	1.274	0.867	0.907	0.841	0.935	0.986
PatchTST-ForecastPFN	5.423	1.811	1.529	1.409	3.719	1.362	1.566	2.152	3.781	2.855
NBEATS-SarSim0	1.830	0.996	0.842	0.757	0.944	0.746	0.818	0.746	0.800	0.807
PatchTST-SarSim0	1.712	0.989	0.828	0.744	0.989	0.737	0.791	0.800	0.802	0.837
MLP-SarSim0	1.961	1.110	0.864	0.800	1.312	0.763	0.868	0.897	0.947	0.891

Table 17: nMASE on GiftEval, weighted aggregation by frequency. Lower values are better.

datasets (Car Parts, Hospital, M4-monthly, Saugeen, US Births), several of which are also used in pretraining: Hospital, Saugeen, US Births, and Car Parts appear in MOIRAI’s pretraining corpus, and Saugeen and US Births in TTM’s. Thus, at A/Q/M frequencies, foundation models operate in a regime where their pretraining distribution is especially close to the test distribution, whereas SarSim0-pretrained models never see these series and are evaluated in a strict zero-shot setting.

Despite this strong advantage for real-data-pretrained models at A/Q/M, SarSim0 backbones remain highly competitive (in fact, best on Monthly split) and are often best at other frequencies. For the sub-hourly and minute-level frequencies (10T, 15T, 5T), PatchTST-SarSim0 attains the best nCRPS on 10T and 15T and is among the top performers on 5T, outperforming both foundation models and per-dataset supervised NBEATS in several cases. At daily (D) frequency, NBEATS-SarSim0 and PatchTST-SarSim0 slightly improve over the best real-data foundation models in nCRPS, while also yielding strong nMASE, indicating that the synthetic curriculum transfers well to operationally important daily horizons. For the weekly bucket (W), GiftEval aggregates eight datasets: Electricity, ETT1, ETT2, Hierarchical Sales, M4-weekly, Saugeen, Solar, and US Births. As summarized in Appendix C, this segment is heavily represented in the pretraining corpora of the real-data foundation models: Electricity, M4-weekly, and Solar are used to pretrain Chronos; Electricity and M4-weekly are used by TimesFM; and M4-weekly, Solar, Saugeen, and US Births are used by MOIRAI. In other words, weekly-series evaluation is favorable to these models, whose pretraining distributions are very close to the test distribution, whereas SarSim0-pretrained backbones remain strictly zero-shot on all eight datasets. Even in this regime, SarSim0 models are competitive: in nCRPS, NBEATS-SarSim0 and PatchTST-SarSim0 (0.649 and 0.656) trail only Chronos-Base/Small (0.621/0.614), and outperform TimesFM, MOIRAI. A similar pattern holds for nMASE, where NBEATS-SarSim0 and PatchTST-SarSim0 (0.807 and 0.837) sit just behind Chronos-Base/Small. This supports the view that SarSim0 does not rely on any single “sweet spot” frequency, but instead it transfers robustly even in settings where foundation models benefit from substantial pretraining overlap with the evaluation datasets.

When we move attention to synthetic pretraining only, SarSim0 shows a consistent advantage over KernelSynth and ForecastPFN for every frequency bucket. The best synthetic model in terms of both nCRPS and nMASE is always either NBEATS-SarSim0 or PatchTST-SarSim0. The gap is especially pronounced at coarse resolutions (A, Q, M) and at fine-grained sub-hourly/minute frequencies. This suggests that on forecasting tasks represented in GiftEval, the SARIMA-based simulator provides a more robust and broadly useful synthetic curriculum than either KernelSynth or ForecastPFN.

	long	medium	short
Chronos-Base	0.721	0.748	0.596
Chronos-Small	0.746	0.743	0.607
MOIRAI-Large	0.598	0.605	0.597
MOIRAI-Small	0.626	0.636	0.666
TTM-R2-Pretrained	0.774	0.816	0.939
TimesFM	0.742	0.748	0.635
 NBEATS	0.809	0.805	0.823
PatchTST	0.527	0.548	0.628
AutoARIMA	1.152	0.990	0.808
 NBEATS-KernelSynth	0.667	0.710	0.710
NBEATS-ForecastPFN	0.994	1.056	1.270
PatchTST-KernelSynth	0.646	0.666	0.696
PatchTST-ForecastPFN	1.137	1.257	1.517
 NBEATS-SarSim0	0.574	0.601	0.612
PatchTST-SarSim0	0.538	0.561	0.592
MLP-SarSim0	0.601	0.641	0.660

Table 18: nCRPS on GiftEval, weighted aggregation by term length. Lower values are better.

Finally, we compare `SarSim0`-pretrained models to the strong per-dataset supervised baselines, `NBEATS` and `PatchTST`. Both `SarSim0` models achieve lower nCRPS than per-dataset counterparts on 7 out of 10 frequencies (10T, 15T, 5T, H, D, M, W). At a few regimes, supervised models retain a small edge, which we see as natural given their direct access to the target train split. Overall, this comparison reinforces that a single `SarSim0`-based pretraining run can match or exceed carefully tuned per-dataset training across wide range of frequencies.

H.3.3 GiftEval Term Split

	long	medium	short
Chronos-Base	1.040	1.041	0.768
Chronos-Small	1.078	1.048	0.780
MOIRAI-Large	0.985	0.961	0.807
MOIRAI-Small	1.035	1.021	0.888
TTM-R2-Pretrained	1.043	1.036	1.005
TimesFM	1.623	1.447	0.823
 NBEATS	1.056	1.036	0.863
PatchTST	0.881	0.859	0.833
AutoARIMA	1.615	1.026	0.935
 NBEATS-KernelSynth	1.069	1.101	0.925
NBEATS-ForecastPFN	1.676	1.660	1.729
PatchTST-KernelSynth	1.022	1.001	0.912
PatchTST-ForecastPFN	1.681	1.666	1.879
 NBEATS-SarSim0	0.923	0.907	0.802
PatchTST-SarSim0	0.896	0.876	0.801
MLP-SarSim0	0.959	0.955	0.871

Table 19: nMASE on GiftEval, weighted aggregation by term length. Lower values are better.

	multivariate	univariate
Chronos -Base	0.685	0.627
Chronos -Small	0.684	0.647
MOIRAI -Large	0.635	0.572
MOIRAI -Small	0.640	0.659
TTM -R2-Pretrained	0.833	0.907
TimesFM	0.717	0.652
NBEATS	0.790	0.837
PatchTST	0.556	0.613
AutoARIMA	1.032	0.826
NBEATS -KernelSynth	0.700	0.700
NBEATS -ForecastPFN	1.113	1.194
PatchTST -KernelSynth	0.683	0.674
PatchTST -ForecastPFN	1.217	1.501
NBEATS - SarSim0	0.594	0.607
PatchTST - SarSim0	0.546	0.595
MLP - SarSim0	0.628	0.655

Table 20: nCRPS on GiftEval, weighted aggregation by variate type. Lower values are better.

In Tables 18-19, we further stratify GiftEval by term length: long (including horizons 720, 900), medium (including horizons 480, 600), and short (including horizons 6, 8, 12, 13, 14, 18, 30, 48, 60). Before discussing the results, it is important to note that, among these three strata, the short-term split is the most affected by pretraining overlap. It contains 28 datasets, of which six are the M4 competition subsets (daily, hourly, monthly, quarterly, weekly, yearly) used to pretrain all real-data foundation models (**Chronos**, **MOIRAI**, **TimesFM**, **TTM**), as documented in Appendix C. In addition, **Chronos** sees three more short-term datasets (Solar, KDD Cup 2018, Electricity); **MOIRAI** sees twelve more (Car Parts, Covid Deaths, Hierarchical Sales, Hospital, Jena Weather, KDD Cup 2018, Loop Seattle, Saugeen, Solar, SZ-Taxi, Temperature Rain, US Births); and **TimesFM** sees Jena Weather and Electricity. Consequently, a substantial fraction of the short-term evaluation split consists of datasets that foundation models have already seen during pretraining, whereas **SarSim0** models see none of them. Despite this favorable overlap for the real-data models, on short-term nCRPS **SarSim0**-pretrained backbones (**PatchTST**-**SarSim0**: 0.592, **NBEATS**-**SarSim0**: 0.612) outperform all foundation models, and on short-term nMASE they are only slightly behind **Chronos**. Across long and medium terms, which are much less affected by leakage, **SarSim0**-pretrained models are noticeably ahead of the foundation models.

When we move attention to synthetic-only pretraining, **SarSim0** clearly dominates the other synthetic baselines across all term lengths. In Tables 18-19, **NBEATS**- and **PatchTST**-**SarSim0** achieve lower nCRPS and nMASE than their KernelSynth and ForecastPFN counterparts in all three splits (long, medium, and short).

H.3.4 GiftEval Variate Type Split

We next stratify GiftEval by variate type (Tables 20-21). The univariate split contains 20 datasets (Car Parts, Covid Deaths, Electricity, Hierarchical Sales, Hospital, KDD Cup 2018, Loop Seattle, M-Dense, M4 Daily/Hourly/Monthly/Quarterly/Weekly/Yearly, Restaurant, Saugeen, Solar, SZ-Taxi, Temperature Rain, US Births). As detailed in Appendix C and Section H.3.3, a large fraction of these are used in pretraining the real-data foundation models (all overlapping datasets are univariate). In contrast, the multivariate split provides a much cleaner zero-shot testbed: to the best of our knowledge, there is no pretrain-test leakage in this segment.

Against this backdrop, **SarSim0**-pretrained backbones are highly competitive on the univariate split: **PatchTST**-**SarSim0** (0.595) and **NBEATS**-**SarSim0** (0.607) lie close to the leading **MOIRAI**-Large (0.572) in nCRPS. In nMASE, **MOIRAI**-Large again leads (0.773), with **NBEATS**-**SarSim0** (0.781) and **PatchTST**-**SarSim0** (0.788)

	multivariate	univariate
Chronos-Base	1.013	0.780
Chronos-Small	1.026	0.797
MOIRAI-Large	1.023	0.773
MOIRAI-Small	1.021	0.890
TTM-R2-Pretrained	1.072	0.980
TimesFM	1.497	0.829
NBEATS	0.998	0.892
PatchTST	0.906	0.805
AutoARIMA	1.318	0.912
NBEATS-KernelSynth	1.098	0.914
NBEATS-ForecastPFN	1.802	1.627
PatchTST-KernelSynth	1.049	0.885
PatchTST-ForecastPFN	1.740	1.825
NBEATS-SarSim0	0.943	0.781
PatchTST-SarSim0	0.904	0.788
MLP-SarSim0	0.979	0.854

Table 21: nMASE on GiftEval, weighted aggregation by variate type. Lower values are better.

essentially matching the best real-data models and improving over the per-dataset PatchTST/**NBEATS** baselines (0.805/0.892).

The picture is even more interesting on the multivariate split, where pretrain-test overlap is much less pronounced. Here, PatchTST-SarSim0 attains the best nCRPS (0.546), ahead of MOIRAI-Large (0.635), Chronos-Base (0.685), TimesFM (0.717), and the per-dataset PatchTST baseline (0.556). Across both variate types, SarSim0-pretrained models consistently outperform their KernelSynth and ForecastPFN counterparts. Taken together, these results indicate that a univariate SARIMA-based simulator can support strong generalization not only to unseen univariate series, but also to multivariate benchmarks, without explicitly modelling cross-series structure.

H.4 Additional ablation comparing SARIMA-only case and AutoARIMA

We define a cleaner experiment here to study the relationship between AutoARIMA and the generalization of models trained on SarSim0 and its components. In particular, Table 22 presents an additional row, in which we study the accuracy of NBEATS trained exclusively on SARIMA process (row SarimaOnly) without the use of Noisers or SARIMA-2. The conclusions remain aligned with our previous observations. On GiftEval, even the SARIMA-only student (**NBEATS-SarimaOnly**) substantially outperforms AutoARIMA (0.672/0.912 vs. 0.940/1.074 in sCRPS/MASE), despite being trained on essentially the same model family. On the M-Series, the picture is more mixed, as before: AutoARIMA remains better in MASE (0.843 vs. 0.869/0.891), while sCRPS is comparable. This is consistent with our discussion that the classical M-Series are particularly favorable to per-series ARIMA/ETS-type models and with our original characterization of this phenomenon as early, domain-dependent evidence rather than a universal effect.

	GiftEval		M-SERIES	
	sCRPS	MASE	sCRPS	MASE
AutoARIMA	0.912	1.074	0.096	0.843
NBEATS-SarSim0	0.602	0.849	0.096	0.869
No SARIMA-2	0.655	0.913	0.104	0.941
No Noisers	0.609	0.856	0.096	0.860
SarimaOnly	0.672	0.940	0.101	0.891

Table 22: Extended ablation on simulator components, including an additional SARIMA-only row (NBEATS-SarimaOnly) trained solely on pure SARIMA samples, without Noisers or SARIMA-2. On GiftEval, this SARIMA-only student already substantially outperforms the practical per-series baseline AutoARIMA in both sCRPS and MASE.